Chapter 7

Comparison of model predictions with observations

Chapter 3 demonstrated that in general there was broad agreement between numerically derived estimates of recent ice-volume changes in mountain glaciers and direct observational data for the small number of glaciers for which such data is available. However, it remained unclear which particular combination of temperature and precipitation data sets provided the best agreement with respect to the observationally based data. Thus, this chapter compares geodetic signals, i.e. relative sea-level changes and vertical displacements, that are predicted numerically with observations at tide gauge, GPS, and VLBI sites. Additionally, the method to determine the mountain glacier contribution to geodetic signals that is used in this thesis is critically assessed by comparing it to results from other studies. A global comparison is presented in Section 7.1 and more detailed regional analyses are presented for Alaska and Svalbard in Sections 7.2 and 7.3, respectively.

7.1   Comparison on a global scale

Section 3.2.1.1 described the method used in this study for determining observational based ice-volume changes of 100 glaciated regions (denoted *D&M compilation*). The observations used in the D&M compilation were available for only a limited number of glaciers, and thus the deduced regional and global ice-volume changes are based on assumptions, i.e. extrapolation and enhancement

methods. The global change in ice volume in the D&M compilation is estimated to be 146.5 km^3 year^{-1} of water, equivalent to 0.40 mm year^{-1} of eustatic sea-level rise, over the period 1961-2003. The resulting predicted geodetic signals and their spatial distribution are discussed in the following sections and compared to the predictions based on the ice-volume changes derived numerically earlier in this thesis.

7.1.1 Predicted geodetic signals caused by observed ice-volume changes

On a global scale, the average change in ice volume over the period 1961-2003 of the D&M compilation is slightly greater than that derived by the numerical approach based on $T_G P_{Z\&O}$ but comparable to that based on $T_{OF} P_{OFseries}$ (see Figure 3.10 on page 99). However, to investigate the effect of the differences in the climate models on the estimates of geodetic signals, numerically derived ice-volume changes based on both data sets, $T_G P_{Z\&O}$ and $T_{OF} P_{OFseries}$ with a global Θ of 0.15 K (see Section 3.1), are used in the calculation as well as the observationally based data set (D&M compilation).

Figure 7.1a shows the spatial distribution of relative sea-level changes applying average ice-volume changes of the D&M compilation determined for the period 1961-2003. The response is calculated on the standard Earth model *ma2A* (Table 4.1 on page 117). The global pattern in Figure 7.1a is comparable to that obtained when using results from the numerical model of mountain deglaciation based on temperature and precipitation data sets for the slightly shorter period of 1961-1990 (see Figures 5.4 and 5.7), i.e. significant relative sea-level changes are concentrated in the same four principal regions (North America, Patagonia, central Asia, and the Arctic Sea). However, locally the geodetic signals vary. For example, the signals in Patagonia and New Zealand are more pronounced when applying the ice-volume changes of the D&M compilation than the estimates derived from the numerical models of mountain deglaciation. This is caused by the smaller ice-volume changes predicted numerically compared to the observational based estimates in those regions (see Tables C.1 and C.2 on pages 330-334). Conversely, the predicted geodetic signals in Iceland using the D&M compilation of mountain deglaciation are smaller than those based on the numerically derived ice-volume changes. Similar local differences exist when comparing the predictions of the spatial distribution of vertical land movements based on the numerical models of
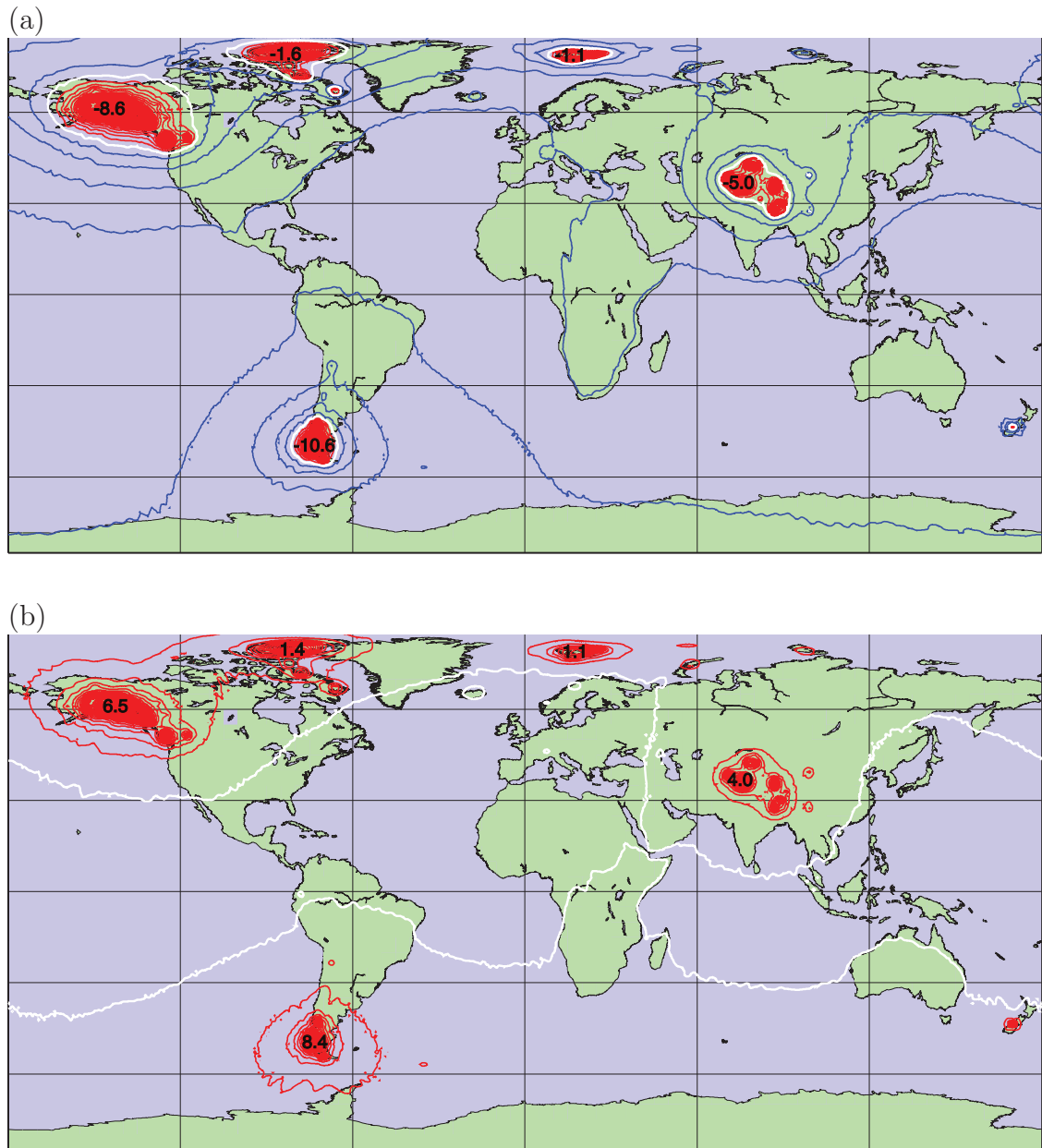
(a)

(b)

Figure 7.1: Spatial distribution of geodetic signals caused by recent mountain deglaciation applying average values of the D&M compilation over the period 1961-2003 (see Figures 7.4 and 7.18 for more detailed plots of Alaska and Svalbard). The response is calculated on the standard Earth model $ma2A$. The contour interval is 0.1 mm year^{-1}. Numbers refer to the local maximum rates in mm year^{-1}. (a) Relative sea-level changes. Red contour lines represent relative sea-level fall, blue contour lines represent relative sea-level rise. White represents the zero contour line (no change). (b) Vertical surface deformation. Red contour lines represent vertical land uplift. White represents the zero contour line.

ice-volume changes (Figures 5.5 and 5.8) with that based on the D&M compilation (Figure 7.1b).

Note that, as already discussed in Section 5.1, the uplift signal is of longer wavelength than the sea-level signal. Therefore, modelling both signals can provide complementary information when explaining the observations. This is also illustrated by comparing the predicted signals using different deglaciation models (see Table 7.1). For example, the predicted vertical land movements at the station Ny Ålesund in Norway using the deglaciation model based on $T_G P_{Z\&O}$ and $T_{OF} P_{OFseries}$ are in good agreement, but for the same site the predicted relative sea-level changes vary by approximately 14%. Another example is the station Resolute in Canada where the sea-level predictions are of very similar magnitude but the estimated surface displacements differ by about 60%.

Predicted relative sea-level changes at PSMSL sites and vertical land movements at GPS sites due to recent mountain deglaciation based on both numerical and observational estimates of ice-volume changes are compared in Table 7.1. Predicted signals of relative sea-level changes at some sites are strongly negative. These sites are located close to the areas of major deglaciation and the signal is dominated by the rebound effect and the change in gravitational potential (see Section 4.3). From the comparison in Table 7.1, similar conclusions as above are drawn: In general, the amplitudes of the predicted geodetic signals at most of the selected sites are greater using the D&M compilation of mountain deglaciation compared to predictions using the ice-volume changes of the numerical models (see also Figure 7.2). This is mainly attributed to the greater global ice-volume loss estimated in the former. However, exceptions occur in regions where the local ice-volume loss derived from the numerical model that is based on temperature and precipitation data sets is predicted to be greater.

Using T_G limits the time frame to the period 1871-1990 for which ice-volume changes, and hence geodetic signals, can be predicted. However, temperature up to the year 2000 is available from the O'Farrell data set data and geodetic signals over the period 1961-2000 are predicted here. Hence, small variations in the three estimates of geodetic signals, listed in Table 7.1, are also expected resulting from the slightly different time period considered in the various models.

Table 7.1 also lists predictions of relative sea-level changes for far-field sites (e.g. Australia, New Zealand). The variations in estimates at these sites between models illustrate the differences in the estimates of global ice-volume changes. This is because the dominant contribution to the signal at these sites is the addition

	Site	$\mathbf{T}_G\mathbf{P}_{Z\&O}$ 1961-1990	$\mathbf{T}_{OF}\mathbf{P}_{OFseries}$ 1961-2000	**D&M comp.** 1961-2003
tide gauge	**Juneau** (Alaska)	-2.13	-1.88	-3.51
	Reykjavik (Iceland)	-0.16	$+0.22$	$+0.36$
	Ny Ålesund (Norway)	-1.19	-1.04	-0.71
	Punta Arenas (Chile)	-0.11	-0.01	-0.36
	Tromso (Norway)	$+0.13$	$+0.27$	$+0.33$
	Resolute (Canada)	$+0.10$	$+0.10$	$+0.07$
	Kanmen (China)	$+0.24$	$+0.32$	$+0.37$
	Sydney (Australia)	$+0.29$	$+0.42$	$+0.46$
	Dunedin (New Zealand)	$+0.28$	$+0.42$	$+0.40$
GPS	**Fairbanks** fair (Alaska)	$+0.37$	$+0.47$	$+0.70$
	Reykjavik reyk (Iceland)	$+0.26$	$+0.07$	-0.02
	Ny Ålesund nyal (Norway)	$+1.02$	$+1.00$	$+0.75$
	Punta Arenas parc (Chile)	$+0.28$	$+0.30$	$+0.51$
	Tromsoe tro1 (Norway)	$+0.032$	-0.001	-0.003
	Resolute reso (Canada)	$+0.056$	$+0.098$	$+0.134$
	Sheshan shao (China)	-0.013	-0.017	-0.016
	Sydney sydn (Australia)	$+0.011$	$+0.010$	$+0.009$
	Dunedin ous2 (New Zealand)	$+0.029$	$+0.027$	$+0.052$

Table 7.1: Predictions of geodetic signals in mm year^{-1} at tide gauge and GPS stations (see Figure 5.3 and Tables D.1 and D.2) due to recent mountain deglaciation using the standard Earth model *ma2A*. Ice-volume changes are derived from the numerical model based on $\mathrm{T}_G\mathrm{P}_{Z\&O}$ and $\mathrm{T}_{OF}\mathrm{P}_{OFseries}$ (with a global Θ of 0.15 K) and from the D&M compilation. Geodetic signals are averaged over the periods 1961-1990, 1961-2000, and 1961-2003.
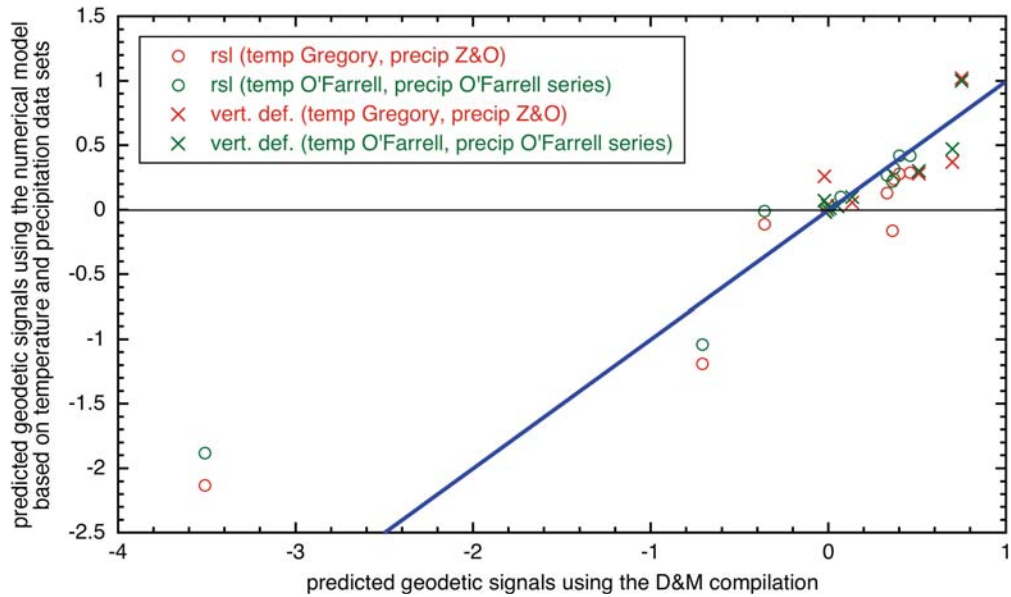

Figure 7.2: Predicted geodetic signals (*rsl* − relative sea-level changes and *vert. def.* − vertical surface deformation) at selected global sites (see Table 7.1) calculated from the numerical model of mountain deglaciation (based on $\mathrm{T}_G\mathrm{P}_{Z\&O}$ and $\mathrm{T}_{OF}\mathrm{P}_{OFseries}$) as a function of the predicted signal using the ice-volume changes of the D&M compilation.

of melt-water and hence predicted relative sea-level changes are similar to the estimated eustatic sea-level change (see Section 4.3).

7.2   Comparison of geodetic signals in Alaska

In the previous section, the global differences between predicted geodetic signals that result from mountain deglaciation derived from different methods are presented. The numerically derived estimates of ice-volume changes and associated geodetic signals are now critically evaluated for the Alaska region (and adjoining Canada) as a whole and also for Southeast Alaska (see Figure 7.3) in the following sections. This is done by comparing the approach and results of this thesis to methods used in previously published studies. This makes it possible to assess the method that is used here for the prediction of geodetic signals and to recalibrate the model (where necessary) to improve the accuracy of results in this study. In this respect, the main focus is on specific regional and local circumstances that consequently result in reassessments of the deglaciation histories in Alaska and particularly of the ice models of the Yakutat Icefield (green dots in Figure 7.3) and the Glacier Bay region (yellow and blue dots in Figure 7.3) as well as the Earth model used.
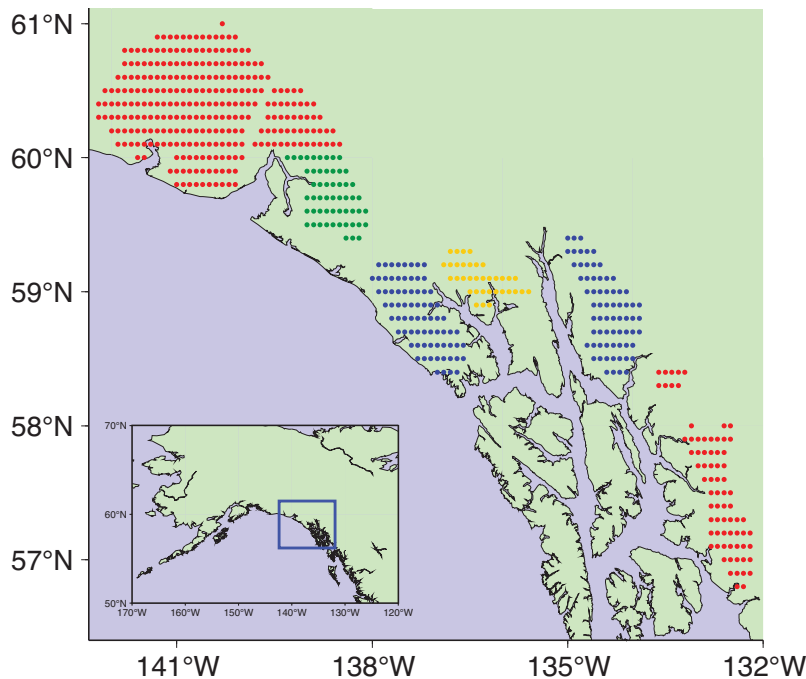

Figure 7.3: Locations and extents of ice cover in Southeast Alaska of the digitised data set (Section 2.3.1.1). Different colours represent different glacier systems discussed in the text of this chapter.

7.2.1 Predicted geodetic signals in Alaska caused by observed ice-volume changes

The spatial distribution of relative sea-level changes and vertical surface deformation in Alaska, as a result of changes in glacial ice volume that are adopted from the D&M compilation, are shown in Figure 7.4. The significantly larger geodetic signal in both plots of Figure 7.4 compared to those using the numerical models of ice-volume changes based on combinations of temperature and precipitation data sets (e.g. Figures 5.11b and 5.14b) is attributed to the larger ice-volume loss of mountain glaciers in Alaska in the D&M compilation. In particular, the ice-volume loss in the D&M compilation is up to ∼1.5 times the value determined by the numerical models.

Predicted estimates of geodetic signals over the time periods 1961-1990, 1961-2000, and 1961-2003 at a few existing tide gauge and GPS stations in Alaska, using the numerical models and the D&M compilation of mountain deglaciation, are listed in Table 7.2. As already noted above, averages over different time periods are unavoidable due to the availability of the various temperature data sets. Compared to the geodetic signals using the D&M compilation, the estimates using the numerical models of mountain deglaciation are consistently smaller (see also Figure 7.5). In particular, estimates at sites closest to the peak of the geodetic signal are about 30-40% smaller (e.g. Skagway, Yakutat, and Whitehorse). Again, this shows the dependence of results on the different predicted ice-volume changes in Alaska, i.e. the ice-volume loss in the D&M compilation is greater than those derived from the numerical model based on combinations of temperature and precipitation data sets. In conclusion, these comparisons show that the use of the different models (numerically derived and observational based) of ice-volume changes can result in differences in the predicted signals that are of an amplitude comparable to the measurement capability of geodetic techniques (Altamimi et al., 2002). Therefore, such measurements have the potential to discriminate between alternative deglaciation models.
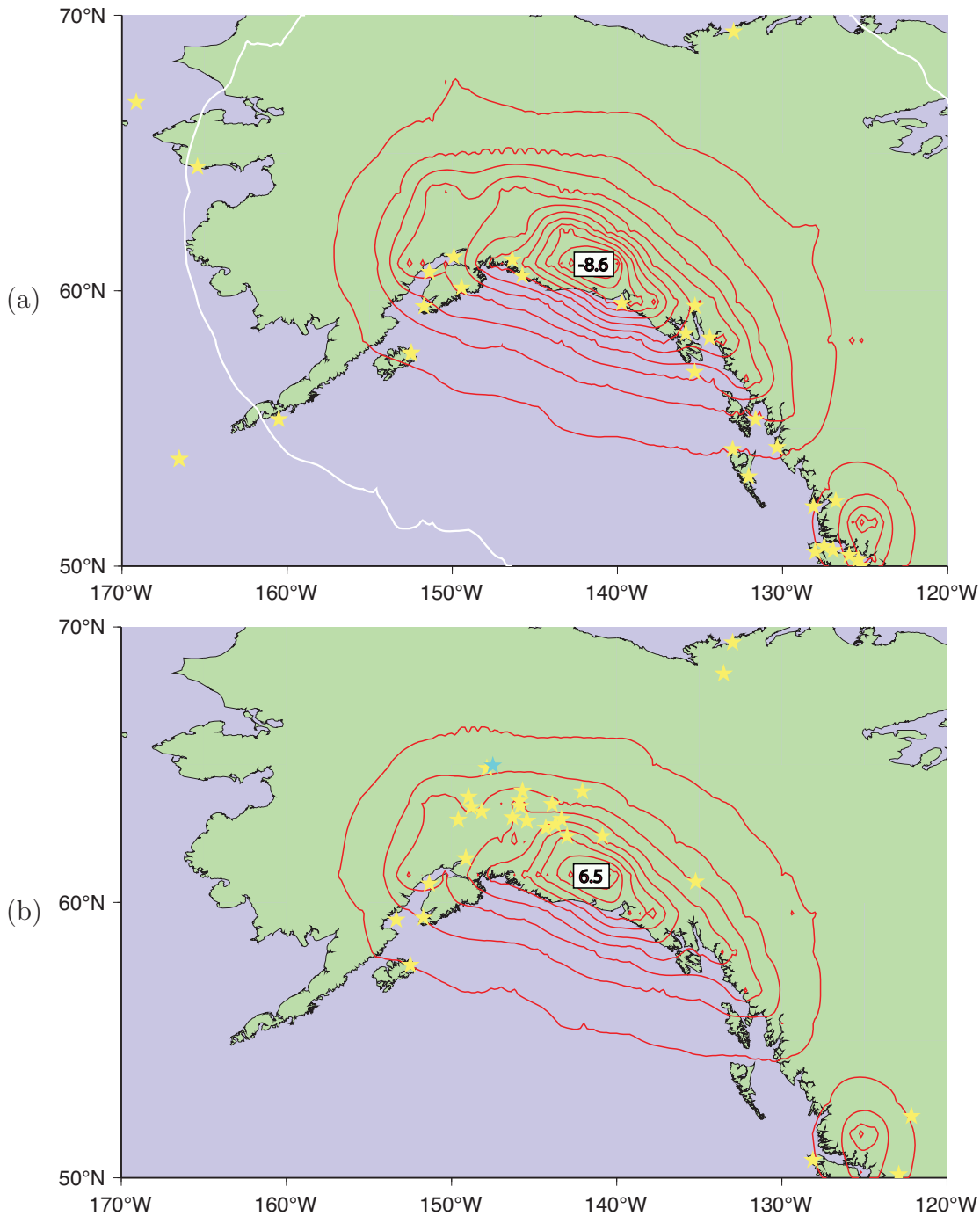
Figure 7.4: Spatial distribution of geodetic signals in Alaska over the period 1961-2003 applying the D&M compilation of recent mountain deglaciation. The response is calculated on the standard Earth model $ma2A$. The contour interval is 0.5 mm year^{-1}. Numbers refer to the local maximum rates in mm year^{-1}. (a) Relative sea-level changes. Red contour lines represent relative sea-level fall. White represents the zero contour line (no change). Stars indicate the locations of tide gauge sites of the PSMSL. (b) Vertical surface deformation. Red contour lines represent vertical land uplift (the outermost contour line represents 0.5 mm year^{-1}). Yellow and blue stars indicate the locations of GPS and VLBI sites, respectively.

	Site	$T_G P_{Z\&O}$ 1961-1990	$T_{OF} P_{OFseries}$ 1961-2000	D&M comp. 1961-2003
tide gauge	**Skagway**	-2.10	-1.96	-3.46
	Yakutat	-3.12	-3.61	-5.46
	Juneau	-2.13	-1.88	-3.51
	Sitka	-0.85	-0.83	-1.55
	Cordova	-2.42	-3.03	-3.72
	Valdez	-3.22	-4.21	-4.80
	Anchorage	-1.23	-1.47	-2.05
GPS	**Fairbanks** fair	0.37	0.47	0.70
	Whitehorse whit	0.82	0.87	1.36
	Palmer atw2	1.44	1.73	2.18
	Refrigerator Rock frig	2.36	2.73	3.46

Table 7.2: Predictions of geodetic signals in mm year^{-1} at tide gauge and GPS stations (see Figures 5.10 and 5.9 and Tables D.1 and D.2) in Alaska due to recent mountain deglaciation using the standard Earth model *ma2A*. Ice-volume changes are derived from the numerical model based on $T_G P_{Z\&O}$ and $T_{OF} P_{OFseries}$ (with a global Θ of 0.15 K) and from the estimates of the D&M compilation. Geodetic signals are averaged over the periods 1961-1990, 1961-2000, and 1961-2003.
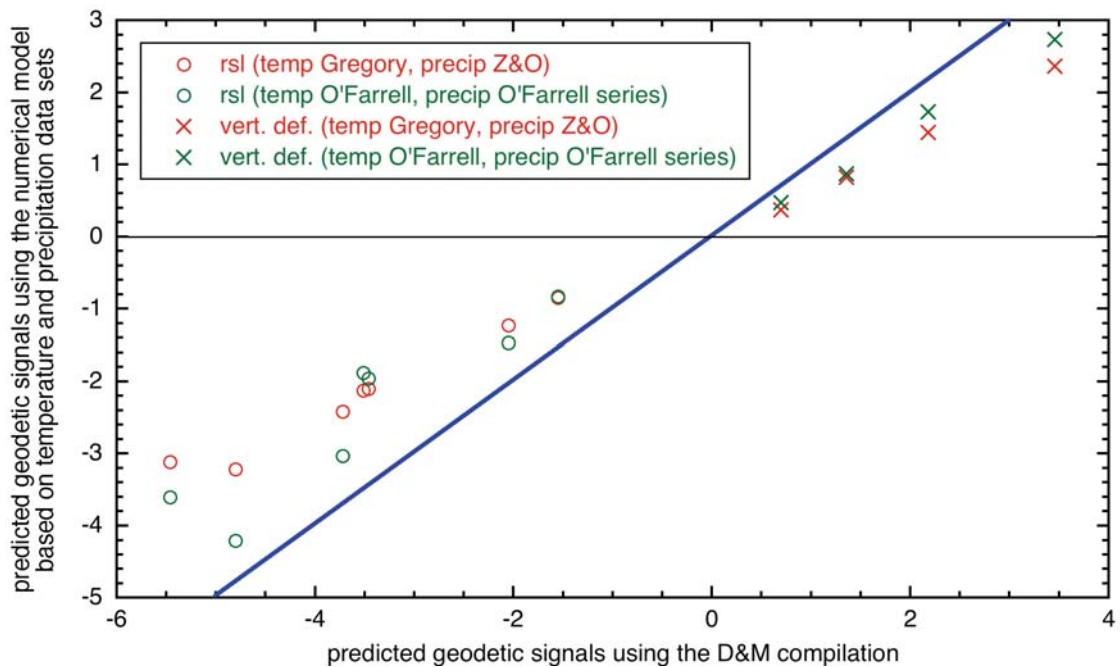

Figure 7.5: Predicted geodetic signals (*rsl* − relative sea-level changes and *vert. def.* − vertical surface deformation) at selected sites in Alaska (see Table 7.2) calculated from the numerical model of mountain deglaciation (based on $T_G P_{Z\&O}$ and $T_{OF} P_{OFseries}$) as a function of the predicted signal using the ice-volume changes of the D&M compilation.

7.2.2 Geodetic signals from the study of Bölling et al. (2001)

The report of Bölling et al. (2001) compared observed sea-level changes and vertical surface deformation in Alaska with estimates derived from modelling of glacial unloading using different Earth models. There are a number of differences between the method used for estimating geodetic signals in the study of Bölling et al. (2001) and that of this thesis. Those discrepancies and the extent to which they affect the results are addressed in this section.

Bölling et al. (2001) developed a *regional* ice model for Southeast Alaska, covering the area between $56°-62°$N and $130°-144°$W (see Figure 7.3), represented by 15 glacier loads that started retreating in 1900. The temporal loading history is derived from a few mass balance measurements. In particular, mean specific mass balance rates over two regions, the *Coast Mountains* and the *St. Elias and Wrangell Mountains*, of -360 and -240 mm year^{-1} were determined and applied to the 15 locations. The total areas of the two regions in Bölling et al. (2001) is 7,398 and 22,557 km^2, similar to those used in this thesis (all but yellow glaciated regions in Figure 7.3). From the glacial areas and mean specific mass balance rates of Bölling et al. (2001) a total ice-volume loss of $\sim$7.4 km^3 year^{-1} w.e. (equivalent to 0.020 mm year^{-1} global sea-level rise) is determined. Dyurgerov and Meier (2005) give an integrated estimate for all Alaskan glaciers and thus it is not possible to extract an estimate for the region of Southeast Alaska alone. The equivalent ice-volume loss for a similar total area as in Bölling et al. (2001) but derived from the numerical model of recent mountain deglaciation using $T_{OF}P_{OFseries}$ is $\sim$4.4 km^3 year^{-1} w.e. (equivalent to 0.012 mm year^{-1} global sea-level rise) over the similar period of 1871-2000. Thus, the rate in ice loss used in Bölling et al. (2001) for the glaciated regions in Southeast Alaska is about 1.7 times that determined here. However, the estimate derived in Bölling et al. (2001) is extrapolated from observations of only a few glaciers and therefore is possibly subject to large uncertainties.

Also note that Bölling et al. (2001) did not account for any recent deglaciation outside Southeast Alaska, whether occurring in the remainder of Alaska or other parts of the world. In contrast, the loading history developed in this thesis is a global deglaciation model and as glaciers occur adjacent to the region of Southeast Alaska, the melting of those are likely to also affect the predicted geodetic signals. Additionally, the local signal of relative sea-level fall, that is mainly a result of glacial isostatic rebound and the change in gravitational potential, is expected to

be partly compensated by the addition of meltwater from glaciers in the far field.

The spatial representation of mountain deglaciation in Southeast Alaska used in Bölling et al. (2001) is also different to that used in this thesis. In particular, the shape of the loads in Bölling et al. (2001) is an ellipse of specified area. In contrast, a digitisation of the extents of glaciated regions in Alaska was undertaken for this thesis (see Section 2.3.1.1). This allows for a more accurate representation of the spatial distribution of glaciers and hence also of their changes in ice volume. Therefore, it is expected that this representation also produces more accurate estimates of geodetic signals (a detailed discussion on the dependence of geodetic signals as a result of different spatial representations of glacier areas was presented in Section 5.2).

Additionally to the ice loads, Bölling et al. (2001) developed three global seven-layer Earth models and several additional regional Earth models in order to account for different possible regional situations (in terms of Earth rheology) in Alaska. The parameters for mantle viscosities and layer thicknesses of one of those models (a mid-range model was chosen) are illustrated in Figure 7.6. Compared to the standard Earth model *ma2A* that was used for most calculations in the previous chapters, the main difference in the Earth model of Bölling et al. (2001) is the higher viscosity in the upper mantle and the lower viscosity in the lower mantle. In order to investigate to what extent the geodetic signals in Alaska due to recent mountain deglaciation are affected when using different Earth models, the model *ma43* (Table 4.2 on page 117) was developed here. It has similar parameters to those suggested by Bölling et al. (2001). The results are shown in columns *2* and *3* of Table 7.3 where predictions of relative sea-level changes at PSMSL sites in Alaska are listed. For this purpose the ice model used (numerical model based on $T_{OF}P_{OFseries}$) remained constant. As already demonstrated in Section 4.3.1.2, variations in estimates of geodetic signals using different three-layer Earth models are negligible and this can be also concluded from the results of this case: on the time scales considered here, the choice of mantle viscosity (at least within the range listed in Table 4.1) is unimportant and a more detailed layering is not required.

Bölling et al. (2001) applied a further 16th load in order to account for an additional retreat in *Glacier Bay* that occurred from 1750 to 1900. This glaciated region is located close to Bartlett Cove (see Figure 5.9) and, due to its time frame, represents the loading history during the LIA (Section 6.3.2). It has an area of 2121 km^2 but further details on the temporal loading history for that glaciated region could not be extracted from the information given in Bölling et al. (2001).
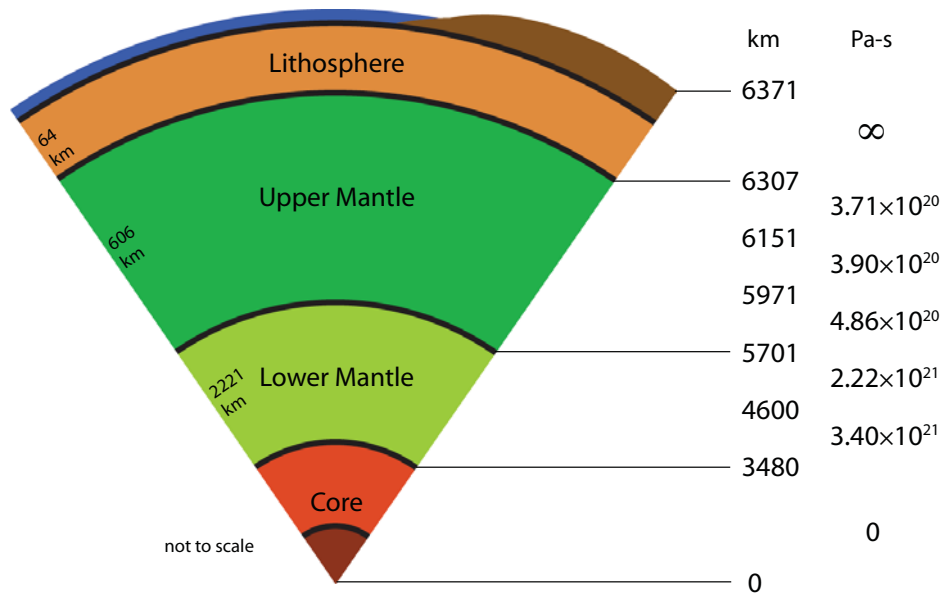
Figure 7.6: Parameters of layer thicknesses and mantle viscosities for the Earth model used by Bölling et al. (2001).

The length of the deglaciation histories used in this thesis generally exclude the period before 1871. However, to investigate the effect on geodetic signals as a result of earlier glacier fluctuations in Glacier Bay, the loading history from 1871 to 2000 (based on $T_{OF}P_{OFseries}$) is extrapolated linearly back to 1750 for a glacial area similar to that of Bölling et al. (2001), represented by the yellow dots in Figure 7.3. Results of relative sea-level changes when applying this earlier load are shown in column 4 of Table 7.3. They illustrate that the earlier deglaciation history developed in this thesis does not affect the estimates of present-day relative sea-level changes significantly.

Another contribution to the geodetic signals considered by Bölling et al. (2001) is the deglaciation following the LGM. For that purpose they used the global ice model ICE-3G of Tushingham and Peltier (1991) representing the deglaciation to the present in time steps of 1000 years. Instead, in Section 6.3.1 a different model of past glaciation/deglaciation cycles, which includes the pre-Holocene Alaskan ice sheets, was presented and is used now in addition to the recent mountain deglaciation (including the extrapolated loading history in Glacier Bay accounting for the glacial fluctuations during the LIA). Resulting predicted relative sea-level changes at existing tide gauge sites in Alaska are listed in columns 5 and 6 of Table 7.3. It was found that on long-term scales different parameters in the three-layer Earth model (in respect to the standard model ma2A) have slightly bigger effects on present-day geodetic signals than in regards to short-term loading

histories. Hence, the Earth model *ma43*, which is similar to that suggested by Bölling et al. (2001), is also used when the response to past glaciation/deglaciation cycles is calculated. Overall, results listed in Table 7.3 demonstrate that for most sites in Southeast Alaska the effect on geodetic signals as a result of the deglaciation following the LGM is relatively small, in particular compared to the effect caused by recent mountain deglaciation, regardless of the Earth model used. Thus, the choice of LGM models is not likely to be important as an uncertainty of 25% in the LGM model results in differences in geodetic signals at these sites of not more than 0.1 mm year^{-1} (i.e. 25% of the difference between columns *4* and *5*, representing the contribution to the geodetic signal due to the deglaciation following the LGM, is mostly less than 0.1 mm year^{-1}).

Modelled results of relative sea-level changes at tide gauge sites derived by Bölling et al. (2001), considering their global (LGM), regional, and Glacier Bay ice models, are listed in column *7* in Table 7.3. Observations of relative sea-level changes (adopted from Bölling et al., 2001) at tide gauge sites in Southeast Alaska are listed in the last column. Observations for the majority of the tide gauge records listed in Bölling et al. (2001, Table 5.1) began between 1900 and 1960, with exception of a few stations where earlier observations from the late 19th century are given. However, the observations listed in Table 7.3 are predominately from the second half of the 20th century (see column *9*). Hence, all estimates of geodetic signals derived here (columns *2* to *6* in Table 7.3) are averaged over the period 1961-2000.

Table 7.3 illustrates that relative sea-level changes determined by Bölling et al. (2001) are considerably smaller (by an order of magnitude) than the estimates derived in this study, whether from recent mountain deglaciation alone, or from the combined effect of recent mountain deglaciation and the deglaciation of LGM ice sheets. As the local mountain deglaciation models are in agreement to within a factor of about 1.7 (see discussion earlier in this section on page 214) this indicates that the discrepancy in the estimate lies in the Earth responses calculation. The results from the models used here have been frequently compared with other records, e.g. for Scandinavia (compare Milne et al. (2004) with Lambeck et al. (1998)), and hence the estimates derived in this thesis are considered to be accurate.

The pattern of sea-level changes derived here and in Bölling et al. (2001) are comparable (compare pattern of contour lines in Figures 7.7b and 7.7c). This pattern suggests that the spatial distribution is mainly caused by the effect of past glaciation/deglaciation cycles (compare with Figure 6.9a on page 184).

	1	*2*	*3*	*4*	*5*	*6*	*7*	*8*	*9*
	Site	num. deglaciation model based on T$_{OFP_{OFseries}}$					Bölling et al. (2001)	obs.	first and last year of avail. obs.
		ma2A	*ma43*	*ma2A + GB*	*ma2A + GB + LGM*	*ma43 + GB + LGM*			
Yakutat		−3.61	−3.51	−3.62	−3.40	−3.12	−0.20	−6	1940, 1999
Skagway		−1.96	−1.91	−1.99	−2.45	−2.67	−0.29	−17	1909, 1999
Bartlett Cove		−1.91	−1.86	−1.95	−2.09	−1.91	−0.19	−40	1938, 1959
Juneau		−1.88	−1.84	−1.90	−2.29	−2.35	−0.24	−13	1911, 1999
Sitka		−0.83	−0.82	−0.83	−0.71	−0.05	−0.12	−3	1938, 1999

Table 7.3: Comparison of relative sea-level changes over the period 1961-2000 in mm year^{-1} at tide gauge sites in Southeast Alaska. The deglaciation history over the period 1871-2000 derived from the numerical model based on T$_{OFP_{OFseries}}$ with a global Θ of 0.15 K. The response is calculated on the Earth models *ma2A* and *ma43*. Column *4* shows the results when an additional loading history over the period 1750-1870 in Glacier Bay (*GB*) is applied and columns *5* and *6* when the glaciation/deglaciation history prior to and following the LGM is also applied. Predicted relative sea-level changes determined by Bölling et al. (2001) are listed in column *7*. Observations at tide gauge sites and the first and last year of available records (information adopted from Bölling et al., 2001) are listed in the last two columns.
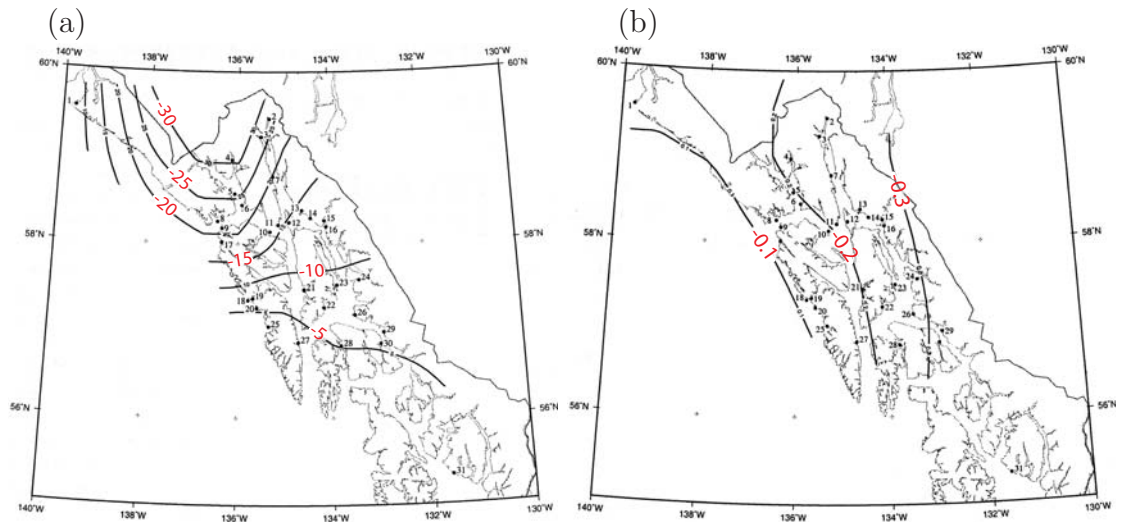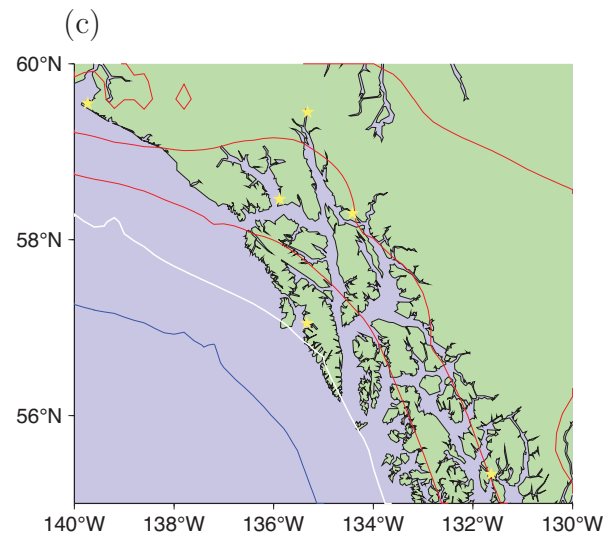
Figure 7.7: Spatial distribution of relative sea-level changes from (a) tide gauge observations and (b) modelled estimates of Bölling et al. (2001) in mm year^{-1}. (c) Predicted relative sea-level changes for the combined solution of the numerical model of recent mountain deglaciation based on $T_{OF}P_{OFseries}$ (with a global Θ of 0.15 K) and the deglaciation following the LIA and the LGM. The response is calculated on the *ma43* Earth model. Red contour lines represent relative sea-level fall, blue represent relative sea-level rise. White represents the zero contour line (no change). The contour interval is 1 mm year^{-1}. Stars indicate the locations of tide gauge sites in Alaska.

Nevertheless, none of the numerically derived estimates adequately explain the present-day observations of sea-level changes (column *8* in Table 7.3). Bölling et al. (2001) noted that their modelled results and the observations mismatch by one or two orders of magnitude. Moreover, the site with the largest observation (i.e. Bartlett Cove) does not correspond with that of the largest modelled estimate (i.e. Skagway) in Bölling et al. (2001). They concluded that glacial rebound isostasy can explain only a small part of the observations (a fraction of a millimetre per year).

Comparing the spatial distribution of relative sea-level changes derived from observations (Figure 7.7a) with that derived numerically in this thesis (Figure 7.7c) shows a considerable difference. This indicates that one or more extra processes have contributed to the geodetic signal in that region and that those need to be investigated to fully understand the observations. Besides the possibility that the derived recent ice-volume loss in Alaska is not adequately estimated, one factor that could accommodate part of an under-estimation of the modelled results is the response due to the loading history during and following the LIA. An attempt to account for this additional loading history within the constraints of the information available was made, but it did not improve the agreement between observations and predictions.

Note that the tide gauge records at the sites in Alaska are sufficiently long (see last column in Table 7.3) to obscure any short-term variations (e.g. meteorological and oceanographic variations) that are not part of the long-term trend (Douglas, 2001). However, a possible factor that contributed to the observed sea-level changes is caused by thermal expansion of the oceans. This correction for thermal expansion is predicted to be somewhere between 0.3 to 2.1 mm year^{-1} over the past century (see Figures 1.1 and 1.2; IPCC, 2001, 2007b), with estimates lying at the higher end of the range predicted for recent decades. However, the warming of the oceans is not globally uniform (see Section 6.5) and in the North Pacific (around 50º to 60ºN) the trend over the second half of the 20th century is predicted to be small, not exceeding 0.8 mm year^{-1}; see Figure 1 in Levitus et al. (2005) and Figure 4 in Antonov et al. (2005). Thus, an adjustment to the above modelled contribution to sea-level changes in Alaska as a result of ocean thermal expansion of less than 1 mm year^{-1} should be applied. Nevertheless, this correction does not improve the agreement between observations and modelled results, and in view of the large rates in observed geodetic signals it may be concluded that the contribution from earlier glacier fluctuations is underestimated by the approach undertaken here. This issue

is addressed in more detail in Sections 7.2.4 and 7.2.5. However, since independent information on the temporal and spatial loading history during and following the LIA are not available at this stage, it was not possible to provide better constraints.

Another process likely to result in geodetic signals, particularly in Alaska, is tectonic activity. As shown in Figure 6.1 on page 167, relative plate movements in the Glacier Bay region are mainly strike slip and consequently vertical crustal movements are expected to be minor compared with further north (in the St. Elias Mountains). Both those issues, i.e. the deglaciation following the LIA and tectonic activity in Alaska, were also briefly discussed in Section 6.1 but a full study is beyond the scope of this thesis.

7.2.3 Geodetic signals from the study of Arendt et al. (2002)

The method used by Arendt et al. (2002) to derive ice-volume changes of mountain glaciers in Alaska was discussed in detail in Section 3.2.4.1, and comparison with the numerical results (based on combinations of temperature and precipitation data sets) indicated major differences. In particular, the ice-volume changes in Alaska derived by Arendt et al. (2002) of -52 and -96 km^3 year^{-1} w.e. for the early and recent periods, respectively, are greater than those determined from the numerical deglaciation model based on $T_G P_{Z\&O}$ and $T_{OF} P_{OFseries}$ (see Table 7.4). T_G is only available until 1996, therefore estimates of ice-volume changes over the recent period are only possible using T_{OF}. Table 7.4 shows that over both periods, the observational estimates are about 1.5 to 1.6 times those determined numerically. This factor of discrepancy has been already found in Section 7.2.1 when analysing the D&M compilation in Alaska, but as the estimate in this compilation is based on the value determined by Arendt et al. (2002), this similarity is not surprising. Note however, that both observationally and numerically derived estimates indicate that the ice-volume loss in the recent period almost doubled compared to that derived over the early period.

Because the Arendt et al. (2002) results are largely based on direct observations of ice-volume changes on some glaciers in Alaska, it could be anticipated that these results are more reliable and therefore appropriate for calibrating the numerical results for Alaska. Although the more recent study by Arendt et al. (2006) showed that the loss from tide water glaciers in Alaska may have been underestimated in Arendt et al. (2002), the latter is an Alaska-wide estimate and is used here. The

	Arendt et al. (2002)	$\mathbf{T}_G\mathbf{P}_{Z\&O}$	$\mathbf{T}_{OF}\mathbf{P}_{OFseries}$
early (1956-1995)	-52 ± 15	-35	-33
	(0.14 ± 0.04)	(0.097)	(0.091)
recent (1996-2000)	-96 ± 35	n/a	-62
	(0.27 ± 0.10)		(0.171)

Table 7.4: Estimates of ice-volume changes in Alaska in km^3 year^{-1} w.e. (equivalent sea-level changes in mm year^{-1} are given in brackets) over the periods 1956-1995 and 1996-2000. Estimates are determined by Arendt et al. (2002) and from the numerical model of mountain deglaciation based on $\mathrm{T}_G\mathrm{P}_{Z\&O}$ and $\mathrm{T}_{OF}\mathrm{P}_{OFseries}$ (with a global Θ of 0.15 K).

approach used to recalibrate the numerically derived ice-volume changes is shown in the following section.

7.2.3.1   Recalibration of the numerical model of recent mountain deglaciation in Alaska

The numerical model for mountain deglaciation contains the parameter Θ that defines the initial imbalance between the glacier and climate state during the reference period (see Section 2.2, Equation 2.3). As discussed earlier, its numerical value is poorly constrained by observational data and it may not be geographically constant (see Section 2.3.5). In particular, it is likely that this parameter is different for maritime environments than for more continental interiors. The attempt to estimate regionally variable Θ values from changes in T_G and T_{OF} within the reference period (see Section 2.3.5) showed that in Alaska the temperature was not increasing significantly more than estimated globally (0.15 K). However, some evidence indicates that the LIA in Alaska may have continued until relatively recent times (see Section 6.3.2). Both Wiles et al. (1999) and Calkin et al. (2001) examined the glacier retreat in Glacier Bay before 1900 and showed that the maximum LIA advance occurred late in the second half of the 19th century and that since then the glaciers have been more or less constantly retreating. Hence, the disequilibrium assumed globally ($\Theta = 0.15$ K) may not be appropriate for Alaska. Using the discrepancy between the results of Arendt et al. (2002) and those from the numerical model provides the possibility to derive a more appropriate Θ value for Alaska.

Changes in ice volume of mountain glaciers in Alaska using the numerical model of mountain deglaciation based on two combinations of temperature and precipitation data sets ($\mathrm{T}_G\mathrm{P}_{Z\&O}$ and $\mathrm{T}_{OF}\mathrm{P}_{OFseries}$) calculated over the early (1956-1995) and

	Θ	$\mathbf{T}_G\mathbf{P}_{Z\&O}$	$\mathbf{T}_{OF}\mathbf{P}_{OFseries}$		Θ	$\mathbf{T}_{OF}\mathbf{P}_{OFseries}$
	0.10	0.092	0.083		**0.10**	0.164
	0.15	0.098	0.091		**0.15**	0.172
	0.20	0.104	0.099		**0.20**	0.180
1956-1995	**0.30**	0.117	0.115	1996-2000	**0.30**	0.196
	0.40	0.130	0.131		**0.40**	0.212
	0.50	0.143	0.147		**0.50**	0.228
	0.60	0.156	0.163		**0.60**	0.244
	0.70	0.169	0.179		**0.70**	0.260
	0.80	0.182	0.195		**0.80**	0.276

Table 7.5: Changes in ice volume of mountain glaciers in Alaska expressed in mm year^{-1} global sea-level rise averaged over the periods 1956-1995 and 1996-2000. Estimates are calculated from the numerical deglaciation model based on $\mathbf{T}_G\mathbf{P}_{Z\&O}$ and $\mathbf{T}_{OF}\mathbf{P}_{OFseries}$ with different values for Θ.
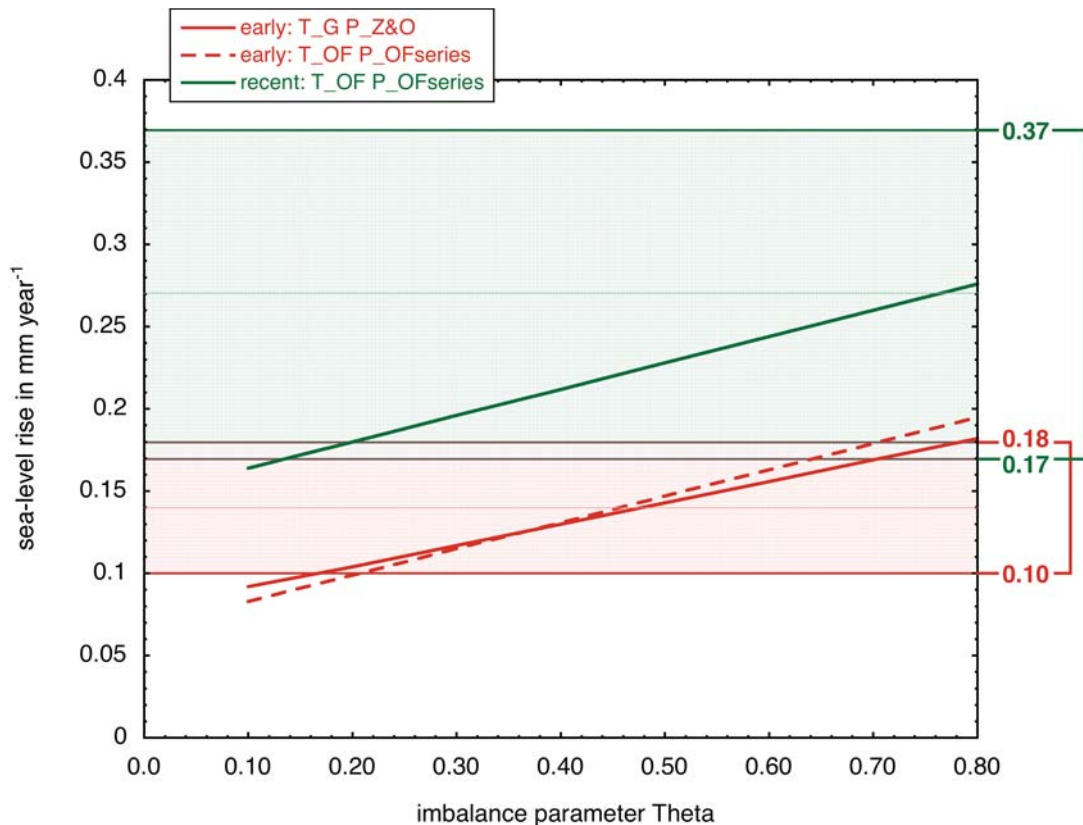
Figure 7.8: Changes in ice volume calculated from the numerical model based on $\mathbf{T}_G\mathbf{P}_{Z\&O}$ and $\mathbf{T}_{OF}\mathbf{P}_{OFseries}$ expressed in mm year^{-1} global sea-level rise as a function of the imbalance parameter Θ for the early and recent periods (see Table 7.5). Red and green highlighted areas cover the estimates for the early and recent periods, respectively, that are derived by Arendt et al. (2002) based on observational data.

recent periods (1996-2000) are listed in Table 7.5. Arendt et al. (2002) determined an ice-volume loss in Alaska equivalent to a global sea-level rise of 0.14±0.04 mm year^{-1} over the early period. Assuming that the only variable in the numerical model is the parameter Θ, the results of Table 7.5 indicate that $\Theta > 0.20$ K and possibly as high as 0.70 K (see also Figure 7.8), and that, therefore, the temperature and glacier state were far from equilibrium before 1900. Only for such high values of Θ do the predicted values of ice-volume loss derived from the numerical model (based on both $T_G P_{Z\&O}$ and $T_{OF} P_{OFseries}$) approach the observed range of 0.10 to 0.18 mm year^{-1} w.e. (see Figure 7.8).

For the recent period of 1996-2000, the numerical predictions match the observed estimate of Arendt et al. (2002) of 0.27±0.10 mm year^{-1} w.e. only if $\Theta > 0.15$ K (for the lower limit) and possibly considerably greater than 0.80 K for the upper limit (see Table 7.5 and Figure 7.8). This is, within the range of the observational uncertainties, not inconsistent with the estimates derived for the earlier interval and overall the comparison indicates that a globally constant value for Θ of 0.15 K, lying at the lower limit of the observational range, is not appropriate for Alaska.

Table 7.6 lists ice-volume changes over the early period of seven smaller-scale regions within Alaska (see Figure 7.9). The first column shows results derived by Arendt et al. (2002). These are compared with ice-volume changes derived numerically based on $T_{OF} P_{OFseries}$. For this purpose the global value for the parameter Θ of 0.15 K is used in columns *4* and *5* and the higher value of $\Theta = 0.50$ K is applied in Alaska in columns *6* and *7*.

Arendt et al. (2002) used an extrapolation method (partly based on a small number of observations, between 1 and 16 glaciers) to derive regional estimates in order to subsequently obtain an Alaska-wide estimate. Using a global value for the parameter Θ of 0.15 K in the numerical model results in estimates for the seven regions that are comparable to the observationally based values, with the exceptions of the regions *Brooks Range* and *St. Elias Mountains* (see Table 7.6). As the former has a small area, this region most likely will not affect the overall picture of volume change in Alaska. In contrast, the ice-volume loss for the St. Elias Mountains determined by Arendt et al. (2002) is very large, i.e. the volume loss is 50% of the total Alaska-wide estimate and about three times the numerically derived value.

In total, the Alaska-wide estimate in Arendt et al. (2002) is about 1.6 times the numerically derived ice-volume loss and this is mainly due to the discrepancy in the estimates for the St. Elias Mountains. However, using a Θ of 0.50 K in Alaska

1		*2*	*3*	*4*	*5*	*6*	*7*
				num. model $\mathbf{T}_{OF}\mathbf{P}_{OFseries}$			
				with $\Theta_{global} = 0.15$ **K**			
Arendt et al. (2002)		**gl#**	**area**	$\Theta_{Alaska} = 0.15$**K**		$\Theta_{Alaska} = 0.50$**K**	
1 Alaska Range	-5.3	8	13,900	-4.14	-4.50	-6.81	-7.56
		10	230	-0.04		-0.07	
		11	960	-0.14		-0.30	
		12	1,250	-0.18		-0.38	
2 Brooks Range	-1.0	7	722	-0.10	-0.10	-0.18	-0.18
3 Coast Range	-5.4	18	10,500	-3.66	-5.55 [a]	-6.27	-9.49 [a]
		19	5,070	-1.89		-3.22	
4 Kenai Mts.	-2.7	13	100	-0.32	-1.63	-0.52	-2.71
		14	4,600	-1.31		-2.19	
5 St. Elias Mts.	-25.7	17	11,600	-5.01	-8.26 [b]	-7.95	-14.68 [b]
		20	10,000	-4.25		-6.73	
6 W. Chugach Range	-6.8	9	800	-0.26	-9.02 [c]	-0.43	-13.98 [c]
		16	21,600	-8.76		-13.55	
7 Kenai Mts.	-1.3	15	8,300	-2.78	-2.78	-4.47	-4.47
4 tide water glaciers	-4.2						
Alaska	$-\mathbf{52.4}$	7-20	89,632		$-\mathbf{31.84}$		$-\mathbf{53.07}$
	(0.145)				(0.088)		(0.147)

[a] includes estimates for tide water glaciers LeConte and Taku
[b] includes estimate for tide water glacier Hubbard
[c] includes estimate for tide water glacier Columbia

Table 7.6: Comparison of ice-volume changes over the period 1956-1995. The first column lists the seven smaller-scale regions within Alaska (see Figure 7.9) and the ice-volume loss in km^3 year^{-1} w.e. determined by Arendt et al. (2002). Columns *2* and *3* list the corresponding glacier numbers and areas in km^2 (Table A.1 on pages 301-304) of the numerical deglaciation model and columns *4* and *6* the corresponding ice-volume loss in km^3 year^{-1} w.e. over the period 1956-1995 using $\Theta = 0.15$ K and $\Theta = 0.50$ K in Alaska. Ice-volume losses in km^3 year^{-1} w.e. of the seven regions in Alaska using $\Theta = 0.15$ K and $\Theta = 0.50$ K are given in columns *5* and *7*. The ice-volume loss of four tide water glaciers (i.e. Columbia, Hubbard, LeConte, and Taku) are derived separately by Arendt et al. (2002) but are included in the numerical estimates in three of the seven regions. Total ice-volume changes for the Alaska region, listed in the last row, are expressed in km^3 year^{-1} w.e. and in mm year^{-1} of global sea-level change (in brackets).
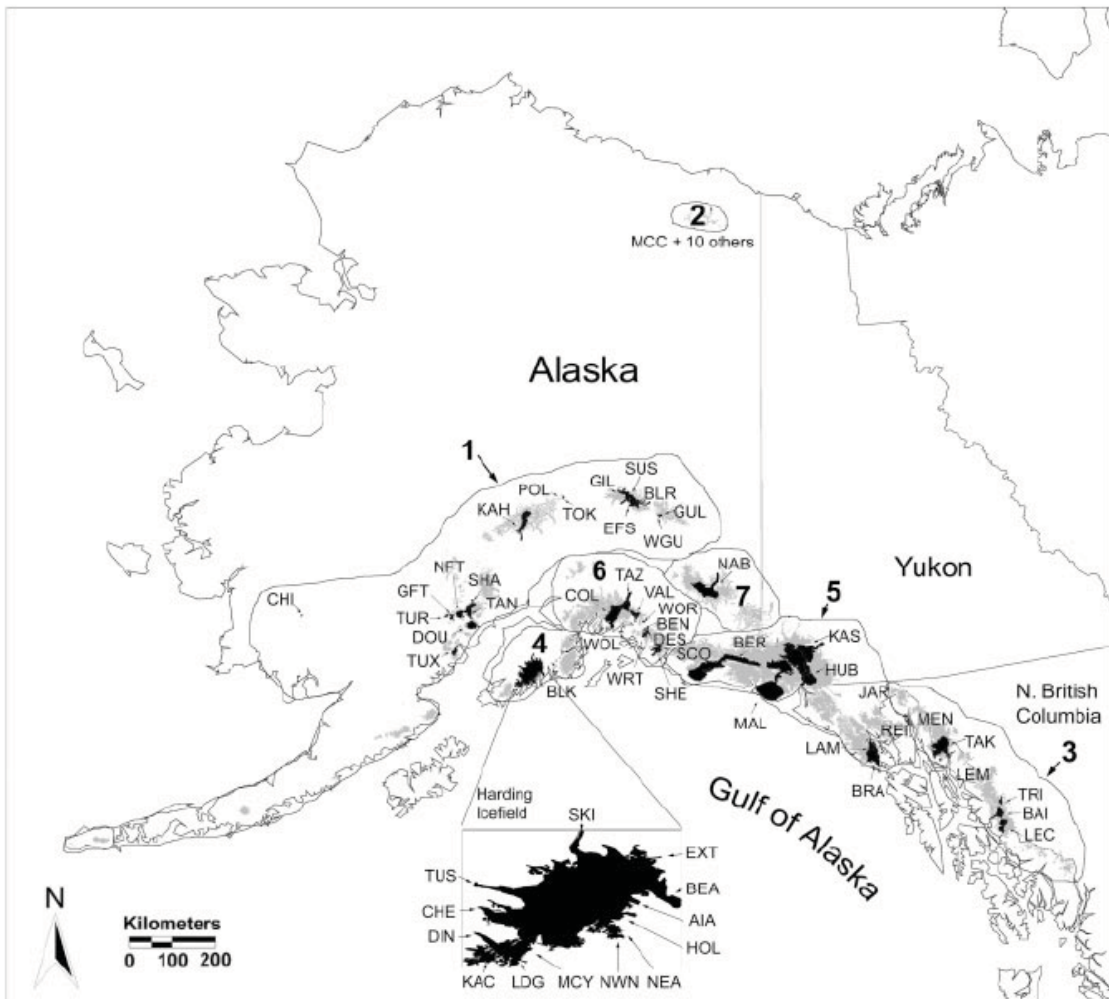
Figure 7.9: Division of seven smaller-scale regions in Alaska defined by Arendt et al. (2002, Figure 1).

produces an estimate for the entire Alaska region that is in agreement with that of Arendt et al. (2002); see last row in Table 7.6. As a consequence of using $\Theta_{Alaska} = 0.50$ K, the calculated ice-volume losses in most of the seven smaller-scale regions are now greater than the observationally based estimates. Using this higher imbalance parameter consequently means that the ice-volume loss in some regions may now be overestimated but the overall picture in Alaska is in agreement with the observationally based estimate of Arendt et al. (2002).

Another question that arises is what are the implications for geodetic signals when using the considerably higher values of recent mountain deglaciation in Alaska. From the above analyses, using a value for Θ of 0.50 K in Alaska in the numerical model produces ice-volume changes comparable to those of Arendt et al. (2002) for the early and recent periods (assuming their mid-range estimates), respectively. The resulting spatial distribution of relative sea-level changes in Alaska over the periods 1956-1995 and 1996-2000 using $\Theta_{Alaska} = 0.50$ K are shown in Figure 7.10.

As already demonstrated in previous sections, variations in local ice-volume changes directly affect the estimates of geodetic signals in that region. Hence, it is unsurprising that the predicted local maximum rates in Figure 7.10 are significantly higher than estimated previously. This can be also seen from the estimates of relative sea-level changes calculated over the periods 1956-1995 and 1996-2000 at a few existing PSMSL tide gauge sites in Alaska listed in Table 7.7. In particular, the results demonstrate that the increase in estimates when using $\Theta = 0.50$ K in Alaska is approximately equivalent to the scaling factor (of ~ 1.5) that is required to be applied to the numerically derived ice-volume losses to match the observational values. This illustrates once more the fact that the accurate determination of loading histories is critical for adequate numerical modelling of geodetic signals. In the absence of more reliable observational and numerical estimates of the mass imbalance and if the crustal response to deglaciation is significant, it may be possible to use the geodetic signals to establish better constraints on the model parameters to be used for extrapolation. The calibrated ice-volume changes in Alaska are used in the following sections presenting a "best estimate" comparison between numerically derived estimates and observations of relative sea-level changes.
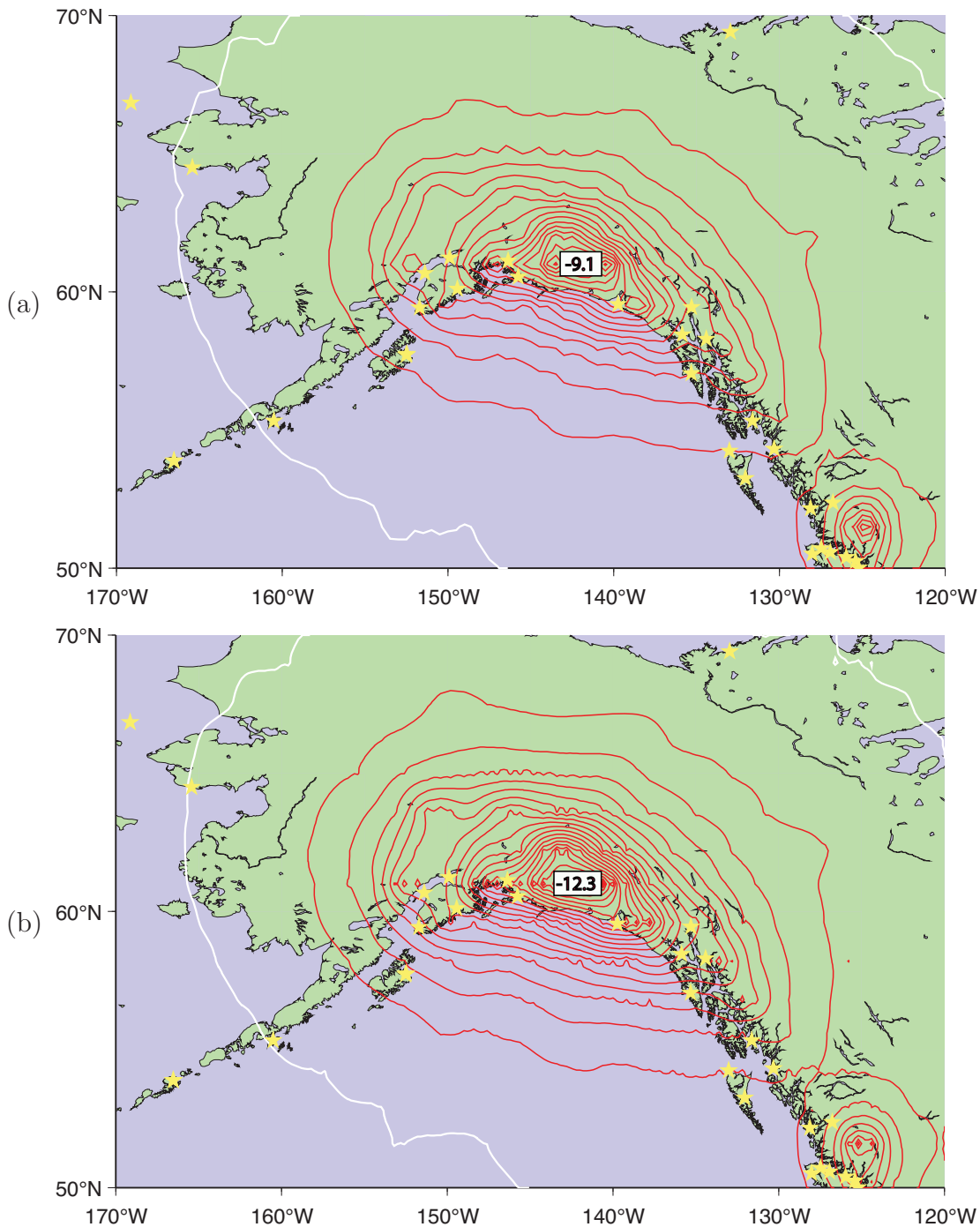
Figure 7.10: Spatial distribution of relative sea-level changes in Alaska over the periods (a) 1956-1995 and (b) 1996-2000 due to recent mountain deglaciation. Ice-volume changes are determined from the numerical model based on $T_{OF}P_{OFseries}$ using $\Theta = 0.50$ K in Alaska and $\Theta = 0.15$ K for all other regions. The response in calculated on the $ma2A$ Earth model. Red contour lines represent relative sea-level fall, white represents the zero contour line (no change). The contour interval is 0.5 mm year^{-1}. Numbers refer to the local maximum rates in mm year^{-1}. Stars indicate the locations of tide gauge sites of the PSMSL.

| Site | num. model $T_{OF}P_{OFseries}$ with $\Theta_{global} = 0.15$ K | | | |
| | 1956-1995 | 1956-1995 | 1996-2000 | 1996-2000 |
	Θ_{Alaska}=0.15 K	Θ_{Alaska}=0.50 K	Θ_{Alaska}=0.15 K	Θ_{Alaska}=0.50 K
Valdez	−3.79	−6.56	−6.13	−8.99
Cordova	−2.73	−4.87	−4.44	−6.68
Yakutat	−3.32	−5.87	−5.16	−7.83
Sitka	−0.80	−1.46	−1.09	−1.77
Skagway	−1.85	−3.34	−2.70	−4.29
Juneau	−1.79	−3.24	−2.54	−4.07

Table 7.7: Predicted estimates of relative sea-level changes over the periods 1956-1995 and 1996-2000 in mm year^{-1} due to recent mountain deglaciation at a few existing PSMSL tide gauge sites in Alaska. Ice-volume changes are calculated from the numerical model based on $T_{OF}P_{OFseries}$ using $\Theta = 0.15$ K. For Alaska Θ was also set to 0.50 K.

7.2.4 Geodetic signals from the study of Larsen et al. (2004)

In view of the poor agreement between observations and numerically derived estimates of geodetic signals in Section 7.2.2 (based on the method of Bölling et al., 2001) and the observations of significantly greater ice-volume losses in Alaska (derived by Arendt et al., 2002, see Section 7.2.3) compared to the numerical model results, a different type of study for Alaska is discussed in this section. Larsen et al. (2004) examined crustal uplift estimates at GPS sites, recent sea-level rates from permanent and temporary tide gauge observations, and total relative sea-level changes from raised shoreline studies in the Glacier Bay region (see Figure 7.3). They compared these observations with predicted values calculated from the Earth's response to mountain deglaciation. They also considered active tectonic deformation in the region as a possible source of the uplift but concluded that this latter deformation was minor, in particular when compared with the rebound signals. This conclusion is consistent with the statement made earlier in this chapter that in Glacier Bay vertical displacements as a result of tectonic activity are small as the relative plate motion is mainly strike slip (see Figure 6.1).

Larsen et al. (2004) developed a *regional* ice model history that is based on ice-volume changes of Arendt et al. (2002). To construct a loading history from the end of the Little Ice Age in Alaska at 1900AD, Larsen et al. (2004) used the estimates for the 1956-1995 period derived by Arendt et al. (2002) for extrapolation. They determined a total ice-volume loss of 5900 km^3 w.e. (equivalent to 16.30 mm global sea-level rise) over the period 1900-2005 (see upper panel in Figure 7.12).

Earlier in this thesis, a numerical deglaciation model over the period 1871-2000 (based on $T_{OF}P_{OFseries}$) has been developed (Section 3.1). It was shown in the previous section that by using $\Theta = 0.50$ K in Alaska, resulting ice-volume changes correspond to the observationally based ice loss determined over the second half of the 20th century (Arendt et al., 2002). Over the period 1900-2000 the numerical model estimates an ice-volume loss of 3053 km^3 w.e. (equivalent to 8.43 mm global sea-level rise). Thus, the ice-loading history in Alaska derived in this study is slightly shorter and the total ice loss is smaller than in Larsen et al. (2004) but the latter is based on a simple extrapolation from results determined for the second half of the 20th century and therefore not inconsistent with the numerically derived estimates. Larsen et al. (2004) used 20 km diameter discs to spatially represent the load changes in Alaska. As the digitisation of the glacial extents in Alaska undertaken for this thesis (see Section 2.3.1.1) is done on a 0.1º grid, this resolution is similar or better to that of Larsen et al. (2004) and hence represent an improved data set (a detailed analysis of the effect the spatial distribution of ice-volume changes has on geodetic signals was given in Section 5.2).

Larsen et al. (2004) developed a viscoelastic three-layer Earth model (lithosphere, asthenosphere, and upper mantle) that accommodated the results of the three observational data sets. The parameters of this Earth model, illustrated in Figure 7.11, have different characteristics to the standard model *ma2A* of this thesis. In particular, Larsen et al. (2004) introduced an additional layer, the asthenosphere, with a viscosity of 1.4×10^{19} Pa-s. From regional-scale isostatic studies (e.g. Sigmundsson, 1991), the effect of a low viscosity asthenospheric layer on model predictions showed that including such a layer produces results that are consistent with the geological evidence. Furthermore, as suggested by Ivins and James (1999), such values for lithospheric thickness and asthenospheric viscosity in 'weak mechanical regimes' are characteristic for tectonically active regions. To investigate the effect on geodetic signals of using Earth models with different layering, the model *mbax4A* (Table 4.2 on page 117), which has similar parameters to that suggested by Larsen et al. (2004), was developed.

Predicted relative sea-level changes at permanent and temporarily installed tide gauge sites in Alaska using the Earth models *ma2A* and *mbax4A* when applying the same deglaciation history (numerical model based on $T_{OF}P_{OFseries}$ with $\Theta_{global} = 0.15$ K and $\Theta_{Alaska} = 0.50$ K) are listed in columns *2* and *3* of Table 7.8. The results demonstrate that the low viscosity asthenosphere can affect predictions by up to 30 to 40%.
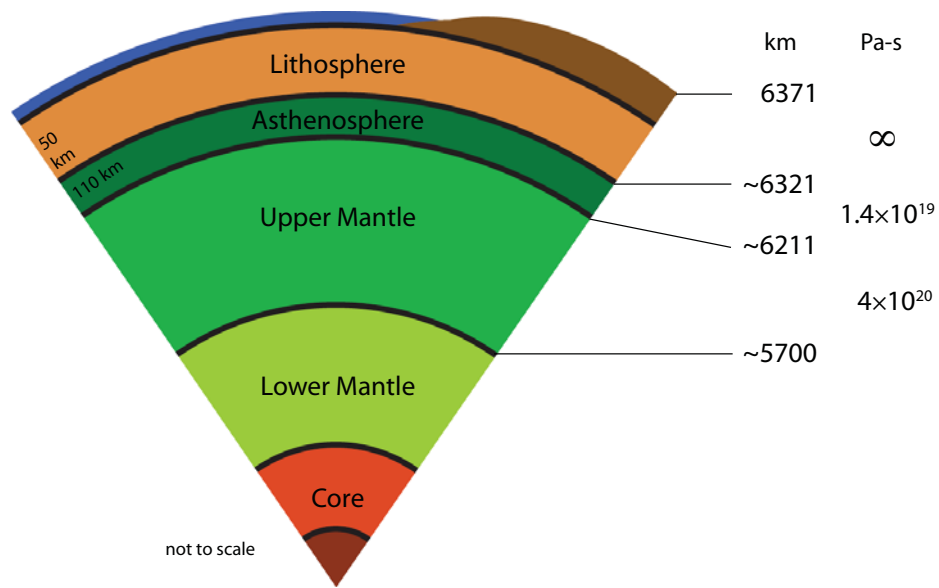
Figure 7.11: Parameters of layer thicknesses and mantle viscosities for the Earth model used by Larsen et al. (2004).

Larsen et al. (2004) applied average thinning rates to all regions in Alaska, except for the Yakutat Icefield where they found that the thickness changes are about three times the regional average. This considerably higher observationally based value was also found when comparison to the numerical derived estimates for smaller-scale regions was made, where the Yakutat Icefield is part of the St. Elias Mountains (see Table 7.6). An average ice-volume loss of 52 km^3 year^{-1} w.e. (Arendt et al., 2002) over an area of 90,000 km^2 results in an average change in ice height of 0.63 m year^{-1}. In a more recent study by Larsen et al. (2007), they found that the Yakutat Icefield lost ice at a rate of up to 8 m year^{-1} with an area-averaged thinning rate of almost 3 m year^{-1} over the second half of the 20th century. The ice-volume loss of the Yakutat Icefield derived numerically in this thesis is estimated to be 2.6 km^3 year^{-1} w.e. over an area of 3421 km^2 (green dots in Figure 7.3), resulting in a thinning rate of 0.83 m year^{-1} over the period 1961-2000, similar to that of the regional average. Using the imbalance parameter for tuning the modelled thinning rate to match the observed value means that Θ has to be set to 3.20 K, a very high value for the imbalance. Another way to consider the observational data in the numerical model and leading to the same results is to simply upscale the thinning rates over the Yakutat Icefield by three which was an easier approach in this case and hence has been done for the following analysis.

Column 4 of Table 7.8 lists estimates of relative sea-level changes in the Glacier Bay region that are caused by recent mountain deglaciation with the thinning rates of

the Yakutat Icefield tripled. The estimate at the tide gauge station located closest to the Yakutat Icefield (site Yakutat) is affected significantly (increase of almost 50%) while estimates at all other sites in the Glacier Bay region increase by less than 20%.

Larsen et al. (2004) additionally determined a regional loading history from ∼1200AD to 1900AD by assigning the advance and retreat stages (based on studies of terminal moraine positions and dendrochronology of overrun trees by Wiles et al., 1999; Calkin et al., 2001) each a percentage of the maximum ice volume in 1900AD. In total, three ice-volume maxima occurred within the LIA (see upper panel in Figure 7.12). A further regional loading model for the period between 300 and 900AD is also determined by Larsen et al. (2004). It was shown in Section 7.2.2, that when extrapolating the last century's loading history linearly back over the past two to three centuries, the resulting present-day geodetic signals are not affected, as the response is primarily elastic. The maximum load-volume in Larsen et al. (2004) was reached within the last one to two centuries. It has been tested whether earlier loading histories (between 300 and ∼1850AD) with smaller volume changes (than the maximum) effect the present-day signals and results showed that the predictions do not vary significantly (in particular with respect to the variations caused by the different ice models over recent times) and therefore such early loading histories were omitted in the analysis of this section.

The separate *Glacier Bay* model in Larsen et al. (2004) represents the extreme ice loss in that area especially from ∼1750 to ∼1950. During that period there was a massive retreat in the glacier systems in Glacier Bay following a 'tidewater glacier cycle' (Meier and Post, 1987; Goodwin, 1988; Motyka, 2003). In particular, Larsen et al. (2004) estimated that the ice-volume loss in Glacier Bay was 2500 km^3 (equivalent to 6.91 mm global sea-level rise) over this 200-year period (see lower panel in Figure 7.12). This is a significant addition to the loss determined over recent periods and to investigate the impact of the melting of this additional massive load on present-day predictions of geodetic signals, a similar ice model located in Glacier Bay with an area of over 11,000 km^2 (blue and yellow dotes in Figure 7.3) reaching back to 1750, was developed for this study. It should be noted here that the spatial distribution of the ice load in Glacier Bay used in Larsen et al. (2004, Figure 9) is different to that of this study. Larsen et al. (2004) inferred the extent of the Glacier Bay model from trimlines, lateral moraines, and terminus moraines of Clague and Evans (1993) with additional data using vertical air photo analysis and field investigations. In contrast, in this thesis the locations and extents
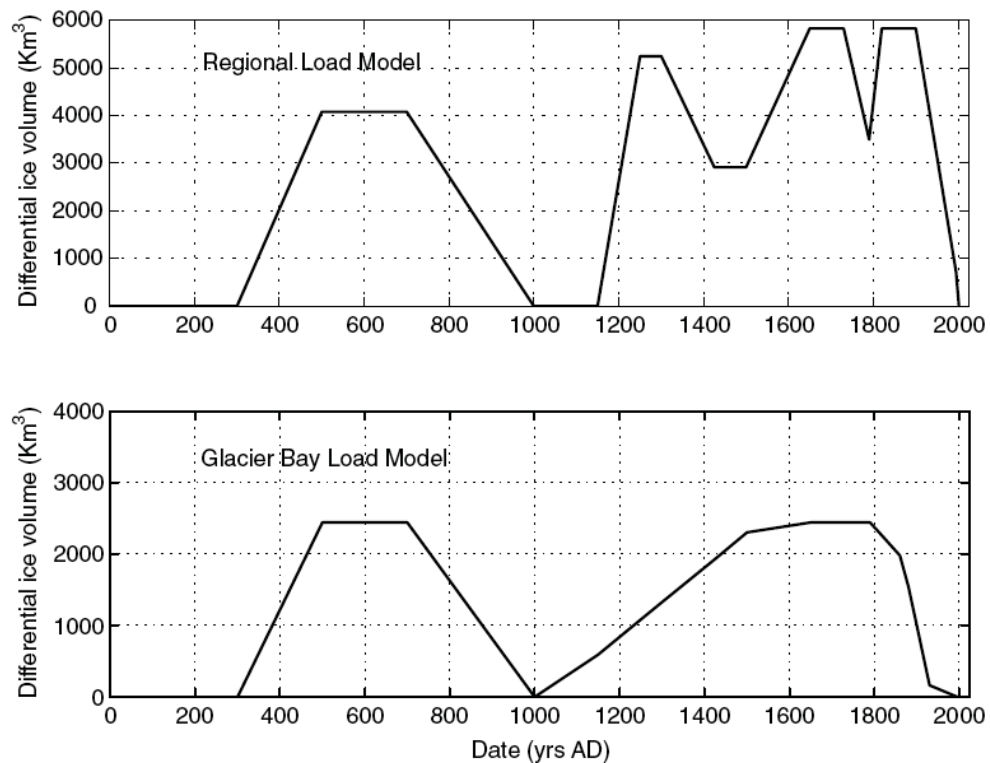
Figure 7.12: Volume changes of regional and Glacier Bay models developed by Larsen et al. (2004, Figure 8).

of the existing glaciers were used, represented by blue and yellow dots in Figure 7.3. As the predictions of geodetic signals are dependent on the spatial distribution of ice-volume changes of nearby glaciers (Section 5.2), the approximation of the glacial extents in this thesis is expected to have an effect on the predictions in the Glacier Bay region but they still provide good first order estimates.

Comparing column *5* with column *2* in Table 7.8 shows the effect on estimates of relative sea-level changes at tide gauge stations when considering the earlier and larger deglaciation history in Glacier Bay. The conclusion is similar to that found for the Yakutat Icefield: predictions at sites located close to the glaciated regions, where the additional load was applied, increase by up to 60%. In contrast, the estimate for the Yakutat station, which is located furthest away of all sites, is less dependent on the additional loading history and the estimate of relative sea-level change increases by only 8%. As expected, the largest impact on relative sea-level changes is predicted in the immediate vicinity of the changing ice loads.

Larsen et al. (2004) did not include the contribution to uplift rates resulting from past melting of the LGM ice sheets, as they note that the uncertainties in the magnitude of this signal are high due to limited knowledge of the ice-sheet history

during the LGM in this area. Larsen et al. (2004) found that the contribution is expected to be small, i.e. 2-4 mm year^{-1}, compared to the observed geodetic signals. This is consistent with the conclusions derived earlier in this chapter (Section 7.2.2) that the melting of past ice sheets (i.e. glaciation/deglaciation cycles prior to and following the LGM) does not significantly affect the predictions in the Glacier Bay area (maximum of 0.5 mm year^{-1}).

Column *6* of Table 7.8 shows relative sea-level changes at tide gauge sites as a result of recent mountain deglaciation, including both the earlier deglaciation history in Glacier Bay as well as the higher melting rate of the Yakutat Icefield over recent periods. Overall, higher rates in relative sea-level changes in the Glacier Bay region of up to 77% are predicted when considering these earlier and greater glacial fluctuations. Column *7* of Table 7.8 lists estimates of relative sea-level changes due to the same recent and early deglaciation histories but applied on the *mbax4A* Earth model. Results demonstrate that this Earth model, with a low viscosity asthenosphere, affects the predictions in such a way that the estimates at the sites are 1.3 to 1.8 times (except for the Sitka site) those when using the *ma2A* Earth model.

Along with four permanent tide gauge stations, records of a further 16 temporary sites (Figure 7.13) were examined by Larsen et al. (2004). Observations at the permanent stations began in the 1940s with more or less continuous records. Measurements at the temporary stations consist of two readings separated by intervals of between 18 and 42 years. For the permanent sites the intervals are sufficiently long to obscure any short-term variations (e.g. meteorological and oceanographic variations) that are not part of the long-term trend (Douglas, 2001), but observations at the temporarily installed sites are less certain which is also reflected in their uncertainties listed in Table 7.8. Observations at 42 temporary GPS sites were undertaken between 1998 and 2002 by Larsen et al. (2004). Data for a further three GPS stations, installed permanently in 1996, 1997, and 2000, were used in Larsen et al. (2004). The onset of emergence of raised shorelines at 14 study sites occurs between the mid 18th and early 19th century and this represents a minimum age for the uplift (Larsen et al., 2004).

Table 7.8 compares the observed relative sea-level changes at a few tide gauge stations in Glacier Bay determined by Larsen et al. (2004) with the modelled values of this study. Since the earliest tide gauge observations in Larsen et al. (2004) began in 1959, calculated geodetic signals in Table 7.8 (columns *2* to *7*) are averaged over the period 1961-2000. For all sites the numerically derived estimates using

1			2	3	4	5	6	7	8
			num. deglaciation model based on $T_{OFP_{OFseries}}$						
			$\Theta_{Alaska} = 0.50$ K			$\Theta_{global} = 0.15$ K			
Site			*ma2A*	*mbax4A*	*ma2A +YI*	*ma2A +GB*	*ma2A +YI +GB*	*mbax4A +YI +GB*	obs.
	°N	°W							
Skagway	59.5	135.5	−3.47	−4.11	−4.08	−5.23	−5.84	−9.24	−17.1±1
Yakutat	59.6	139.7	−6.18	−7.91	−9.11	−6.68	−9.62	−12.77	−13.7±1
Juneau	58.3	134.4	−3.34	−4.35	−3.53	−4.84	−5.04	−7.85	−13.6±1
Sitka	57.1	135.3	−1.49	−0.84	−1.73	−1.92	−2.17	−0.11	−3.0±1
Muir Inlet	58.9	136.1	−4.64	−6.30	−5.18	−6.94	−7.48	−13.52	−26±3
Willoughby Island	58.6	136.1	−4.08	−5.42	−4.68	−6.23	−6.82	−12.12	−23±5
Excursion Inlet Sth	58.4	135.4	−3.24	−4.12	−3.74	−5.08	−5.58	−9.60	−17±3
Lituya Bay	58.6	137.6	−4.74	−5.93	−5.37	−6.62	−7.25	−11.53	−17±3
William Henry Bay	58.7	135.2	−4.06	−5.47	−4.61	−6.14	−6.69	−11.83	−14±5
Swanson Inlet	58.2	135.1	−2.66	−3.13	−2.96	−4.17	−4.47	−6.99	−14±6
Salt Lake Bay	58.0	135.7	−2.03	−1.84	−2.36	−3.26	−3.59	−4.61	−14±7
Auke Bay	58.4	134.7	−3.44	−4.49	−3.69	−5.10	−5.35	−8.71	−12±3
Annex Ceek	58.3	134.1	−3.49	−4.64	−3.66	−4.91	−5.09	−7.76	−10±3

Table 7.8: Predicted relative sea-level changes in mm year^{-1} over the period 1961-2000 at selected tide gauge stations in Glacier Bay, Alaska (see Figure 7.13) as a result of recent mountain deglaciation derived from the numerical model based on $T_{OFP_{OFseries}}$ with $\Theta = 0.50$ K in Alaska and $\Theta = 0.15$ K everywhere else. The higher melting rate of the Yakutat Icefield (*YI*) are applied in columns *4* and *6* and the additional deglaciation history from 1750-1870 in Glacier Bay (*GB*) is applied in columns *5* and *7*. The response is calculated on the *ma2A* and *mbax4A* Earth models. The last column lists observed rates of relative sea-level changes in mm year^{-1} determined by Larsen et al. (2004). The first 4 sites are permanent tide gauge stations from the PSMSL, the remaining are temporarily installed stations.
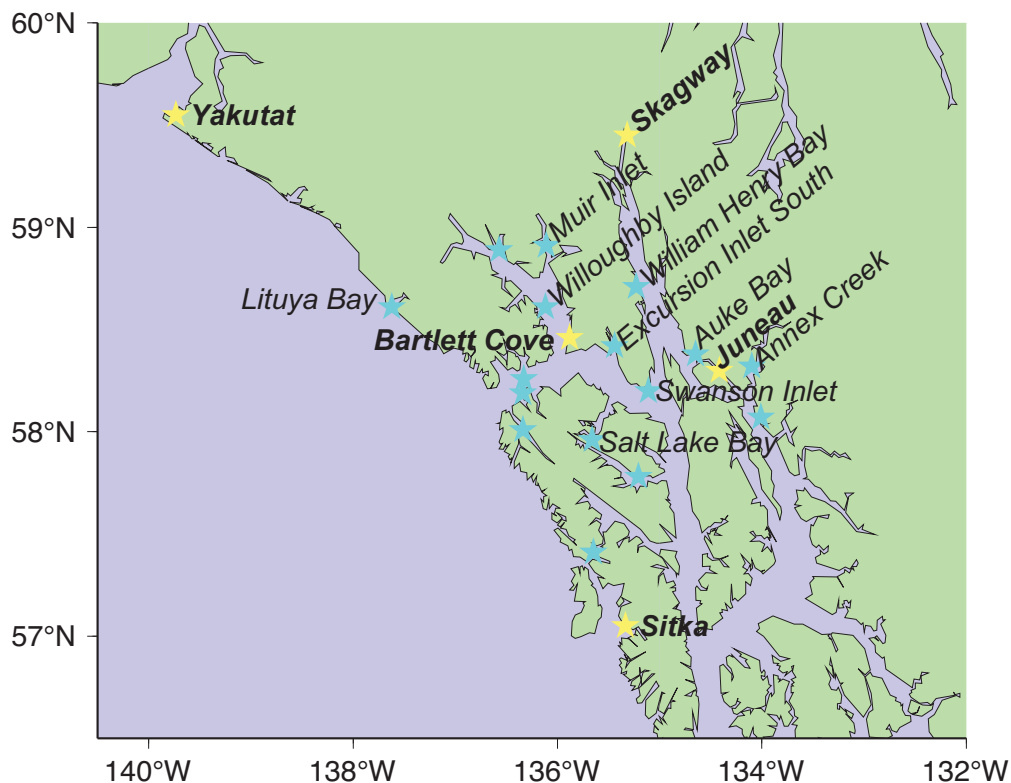
Figure 7.13: Locations of tide gauge stations in Glacier Bay, Alaska, referenced in this section. Yellow and blue stars separate between permanent and temporarily installed sites.

the Earth model *ma2A* are smaller than the observations, even when considering the earlier deglaciation history in Glacier Bay and the increased melting rate over recent decades of the Yakutat Icefield (column *6*). However, using an Earth model with a low viscosity asthenosphere (column *7*) brings the predictions within the range of uncertainties of the observations at a few sites.

The spatial distribution of changes in relative sea level observed at tide gauge sites and vertical surface deformation from GPS observations in Glacier Bay determined by Larsen et al. (2004) are shown in Figure 7.14. The tide gauge data show a peak in upper Glacier Bay, with a maximum of 26 mm year^{-1} relative sea-level fall. This is similar to the earlier study in this region by Hicks and Shofons (1965) using tide gauge observations from the end of the 19th century. In addition to the peak in Glacier Bay, Larsen et al. (2004) found that the GPS uplift rates show another even larger peak of 34 mm year^{-1}, centred over the Yakutat Icefield.

A comparison of the pattern of geodetic signals determined by Larsen et al. (2004) (Figure 7.14) with those derived in this thesis (Figure 7.15) shows that the former are approximately 2 times greater in magnitude. Furthermore, the detailed spatial
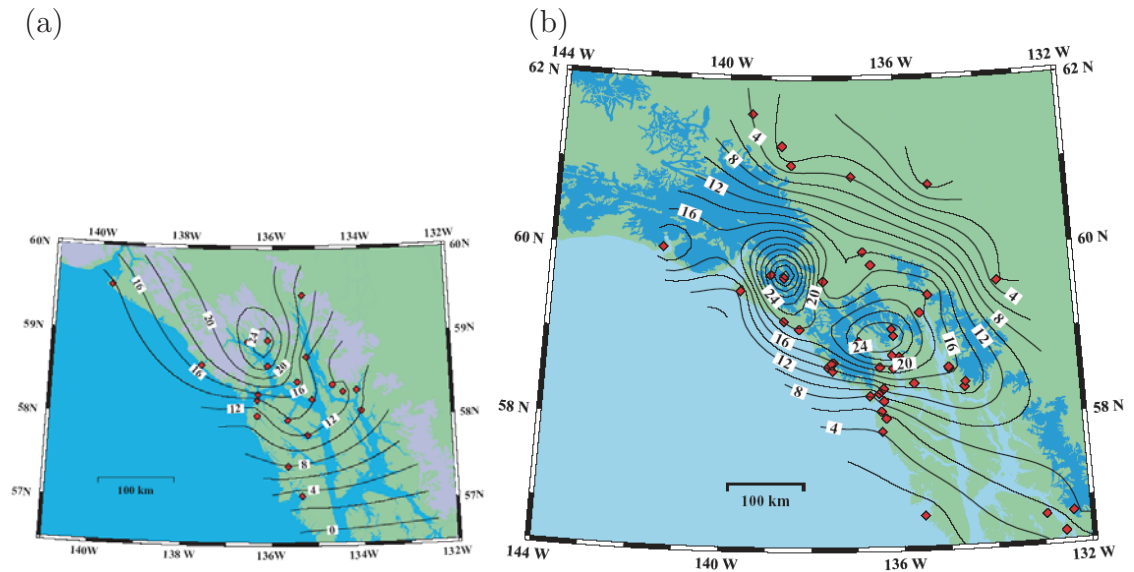
(a)   (b)

Figure 7.14: (a) Rates of relative sea-level fall from tide gauge data determined by Larsen et al. (2004). The contour interval is 2 mm year^{-1} (note that contour lines have been extrapolated significantly beyond the observational sites). Red diamonds indicate tide gauge sites and glaciers are shown in light purple. (b) GPS uplift rates from Larsen et al. (2004). The contour interval is 2 mm year^{-1}. Red diamonds indicate GPS sites and glaciers are shown in dark blue.

(a)   (b)
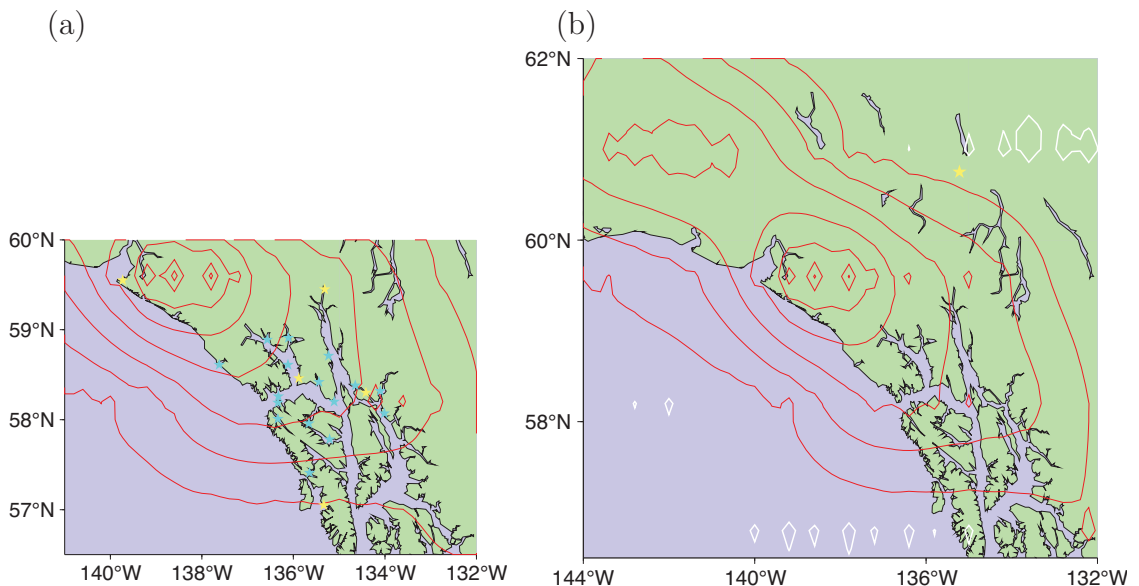
Figure 7.15: Spatial distribution of geodetic signals over the period 1961-2000 in Glacier Bay, Alaska, due to recent mountain deglaciation derived from the numerical model based on $T_{OF}P_{OFseries}$ with $\Theta_{Alaska} = 0.50$ K. The higher melting rate over the Yakutat Icefield and the additional deglaciation history from 1750-1870 in Glacier Bay are applied. The contour interval is 2 mm year^{-1}. The response is calculated on the *mbax4A* Earth model. (a) Red contour lines represent relative sea-level fall (outermost contour line is -2 mm year^{-1}). Yellow and blue stars indicate the locations of permanent and temporary tide gauge stations. (b) Red contour lines represent vertical land uplift (outermost contour line is 2 mm year^{-1}). The star indicates the location of a GPS site.

variability from Figure 7.14 is only partly reproduced in Figure 7.15, which mainly shows a pronounced peak over the Yakutat Icefield. One reason for the different results is likely to be the approximation of the spatial and temporal deglaciation history in Glacier Bay during and following the LIA made in this study (as the required details were not available). Furthermore, the numerical model developed in this thesis also includes mountain deglaciation occurring in other parts of the world which generally has the opposite effect to that of the local geodetic response. Another explanation for the differences in detailed spatial variability may be the lower resolution of the input data, i.e. the maximum spherical harmonic degree is 256 (see Section 4.3). Thermal expansion of the oceans can also contribute to observed sea-level changes. However, as discussed in Sectiion 7.2.2, in Alaska the correction over the second half of the 20th century is estimated to be small (less than 1 mm year^{-1}) and therefore does not improve the agreement between observations and modelled results greatly.

Note that the estimates listed in Table 7.8 and illustrated in Figure 7.15 are averaged over the period from 1961 to 2000. If observations were made over a shorter period, especially over more recent years (e.g. last decade) where considerably increased ice-volume losses were found (as determined by Arendt et al., 2002), the predicted geodetic signal would increase correspondingly. Thus, it is important to use the same time period in order to make adequate comparisons between observations and numerically derived geodetic signals.

7.2.5   Geodetic signals from the study of Larsen et al. (2005)

Larsen et al. (2005) did a follow up study on the rapid uplift rates in southern Alaska. They analysed a GPS network of 72 stations, surveyed primarily in campaign-style 2 to 5 times each over a 5-year period, and compared these observations with modelled results. Differences in the 2005 analyses to Larsen et al. (2004) include the loading history for the Glacier Bay area. In particular, additional observations to constrain the ice-volume loss of the Glacier Bay model in Larsen et al. (2005) lead to a considerable increase of more than 20% to 3030 km^3 (equivalent to 8.37 mm global sea-level rise), compared to the 2004 analyses. This ice loss since 1770 in Glacier Bay alone is equivalent to a global rise in sea level of 8 mm (Larsen et al., 2005).

Following the approach in the previous section, estimates of recent mountain deglaciation over the period 1871-2000 are derived from the numerical model based on $T_{OF}P_{OFseries}$ with $\Theta_{Alaska} = 0.50$ K. The ice-volume loss of the Yakutat Icefield (green dots in Figure 7.3) is tripled and a separate ice model for Glacier Bay was developed over the period 1770-1870 covering an area of over 11,000 km^2 (blue and yellow dots in Figure 7.3). Larsen et al. (2005) also accounted for the possible effect on geodetic signals as a result of the melting of past ice sheets (LGM). However, as shown in Section 7.2.2, the effect on present-day geodetic signals from this source is very small (less than 0.5 mm year^{-1}) in Glacier Bay and hence is omitted here.

With their established loading histories of the regional and Glacier Bay ice models, Larsen et al. (2005) used a range of different Earth models in order to match the observations of land uplift in the Glacier Bay area. Hence, they drive the predictions of vertical uplift rates in Glacier Bay to match the observations. The parameters for layer thicknesses and viscosities of their best fit Earth model are illustrated in Figure 7.16. Compared to the Earth model determined in Larsen et al. (2004), the viscosity of the asthenosphere is lower by one order of magnitude. As in earlier analyses in this chapter, the Earth model *maau4A* (Table 4.2 on page 117) is used for comparison purposes with parameters similar to those suggested by Larsen et al. (2005).
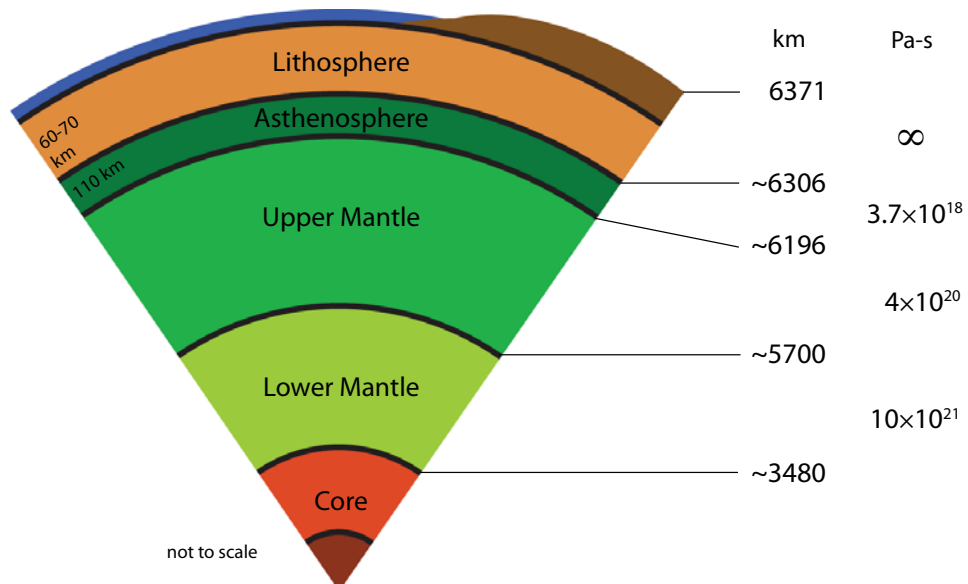

Figure 7.16: Parameters of layer thicknesses and mantle viscosities for the Earth model used by Larsen et al. (2005).

Larsen et al. (2005) accounted for a global sea-level rise of 1.8 mm year^{-1} (Douglas, 1997) over the last 120 years. This observationally based global sea-level rise is
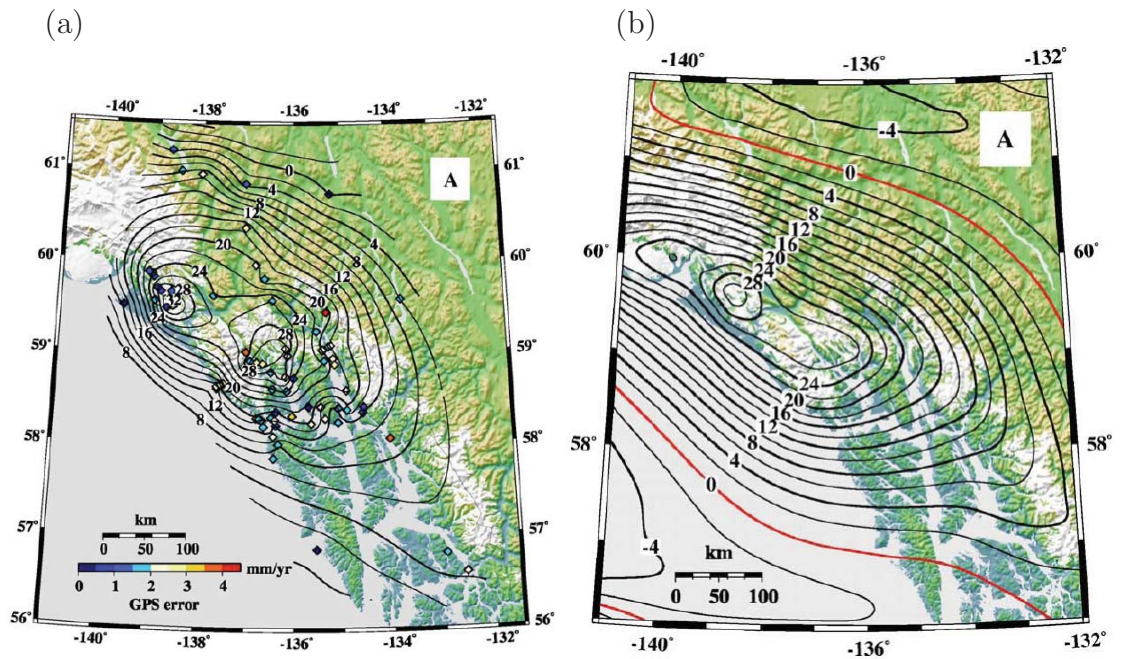
(a)

(b)

(c)

Figure 7.17: Spatial distribution of land uplift rates in Glacier Bay in mm year^{-1} derived from (a) GPS observations, (b) modelled results from Larsen et al. (2005) and (c) numerical model of recent mountain deglaciation (based on $T_{OF}P_{OFseries}$ with $\Theta_{Alaska} = 0.50$ K) and including the higher melting rate of the Yakutat Icefield and the earlier deglaciation model in Glacier Bay. The response is calculated on the $maau4A$ Earth model. Uplift rates are averaged over the period 1991-2000. Red contour lines represent vertical land uplift. White represents the zero contour line (no change). The contour interval is 2 mm year^{-1}.
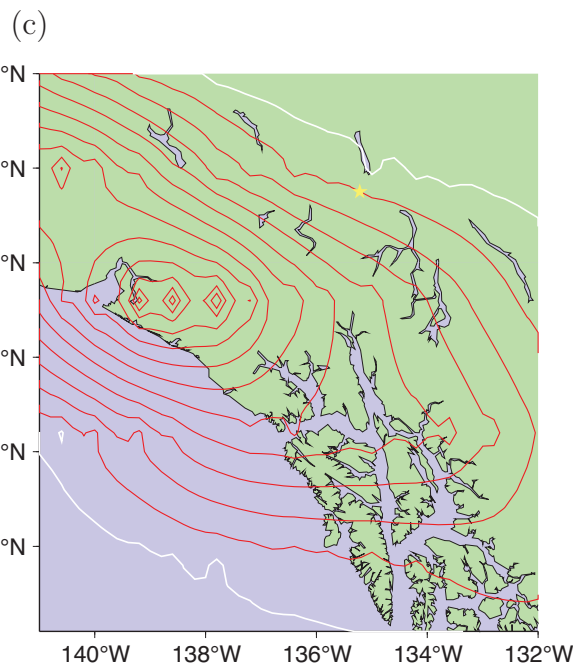
primarily a result of thermal expansion of the oceans and the addition of meltwater from continental ice masses. As the deglaciation model developed in this thesis is a global model, the latter component of global sea-level rise is accounted for (except for any contributions from the Antarctic and Greenland ice sheets). As already discussed in Section 7.2.2, the correction for thermal expansion is predicted to be somewhere between 0.3 to 2.1 mm year^{-1} over the past century but the warming of the oceans is not globally uniform (see Section 6.5). Ishii et al. (2006) estimated a trend in thermal expansion of less than -1 mm year^{-1} over the period 1993-2003 (see Figure 5.15(b) in Bindoff et al., 2007). Although this estimate is subject to uncertainty as it is interpolated, the trend definitely lies between 0 and -3 mm year^{-1}. Thus, the correction used in Larsen et al. (2005) is probably too large and the contribution to sea-level changes in Alaska as a result of thermal expansion of the oceans is adopted from the estimates of Levitus et al. (2005) and Antonov et al. (2005) of less than 1 mm year^{-1}.

Figure 7.17a shows the pattern of vertical land uplift in Glacier Bay determined from GPS observations. The main uplift peak is centred over the Yakutat Icefield and an additional peak in uplift rates occurs in upper Glacier Bay, similar to the pattern derived in Larsen et al. (2004). At some GPS stations uplift rates of more than 30 mm year^{-1} were measured. The pattern of uplift rates is consistent with sea-level observations, however using GPS observations provides a vastly improved picture of the spatial distribution of land uplift. The modelled result of vertical land uplift derived by Larsen et al. (2005) is shown in Figure 7.17b and shows overall similarity to the observations (Figure 7.17a).

Figure 7.17c illustrates the spatial distribution of vertical land uplift in Glacier Bay applying the Earth model and the deglaciation histories derived in this thesis. Averages over the period 1991-2000 are presented to accommodate the short observation period of the GPS measurements. It shows some similarities in the spatial distribution of surface deformation to that derived by Larsen et al. (2005, Figure 7.17b) and hence also to that determined from observations (Figure 7.17a). However, the magnitude of land uplift derived in this thesis is only about half the observational value. This conclusion is also reached in Section 7.2.4, and it is likely that these smaller rates result from the same causes found there, e.g. inadequate representation of the melting of large ice masses in Glacier Bay over the last two to three centuries.

7.3   Comparison of geodetic signals in Svalbard

Section 3.2.4.2 showed that the numerical predictions of ice-volume changes and the observational estimate of the D&M compilation in Svalbard are comparable for the past few decades (see Figure 3.12 on page 106), especially when the numerical model is based on T_{OF} and a global Θ of 0.15 K is applied. This section now investigates whether numerically derived geodetic signals as a result of recent mountain deglaciation are also comparable to the observations of relative sea-level changes and vertical land movements in Svalbard. A detailed discussion for this region including an independent study is presented below for further assessment.

7.3.1   Predicted geodetic signals in Svalbard caused by observed ice-volume changes

Average ice-volume changes over the period 1961-2003 using the D&M compilation have been used to calculate geodetic signals in Svalbard using the standard Earth model *ma2A*. The spatial distributions of relative sea-level changes and of vertical surface displacements are shown in Figure 7.18. Maximum local rates of 1.1 mm relative sea-level fall and vertical land uplift are predicted.

Table 7.9 lists estimates of relative sea-level changes due to recent mountain deglaciation at the two existing tide gauge stations in Svalbard over the periods 1961-1990, 1961-2000, and 1961-2003. Ice-volume changes of the numerical models (based on $T_G P_{Z\&O}$ and $T_{OF} P_{OFseries}$, both with a global Θ of 0.15 K) and the D&M compilation were applied. Using the same deglaciation models, vertical surface deformation at the GPS and VLBI station in Svalbard have been calculated and a comparison of predicted uplift rates is shown in the last row of Table 7.9.

Regardless of the deglaciation model used, the predicted rates of geodetic signals are small. However, the results in Table 7.9 also show that when applying the numerical models of mountain deglaciation (based on $T_G P_{Z\&O}$ and $T_{OF} P_{OFseries}$), the estimated relative sea-level changes at the tide gauge stations in Svalbard are greater compared to the estimates derived when using the D&M compilation (see also Figure 7.19). This may be surprising as the applied ice-volume loss in Svalbard in the numerical model based on $T_{OF} P_{OFseries}$ is 6.89 km^3 year^{-1} w.e. (equivalent to 0.019 mm year^{-1} global sea-level rise), and only slightly greater than that of the D&M compilation (6.05 km^3 year^{-1} w.e. or 0.017 mm year^{-1} global sea-level rise); see also Figure 3.12 on page 106. Nevertheless, the difference illustrates once more
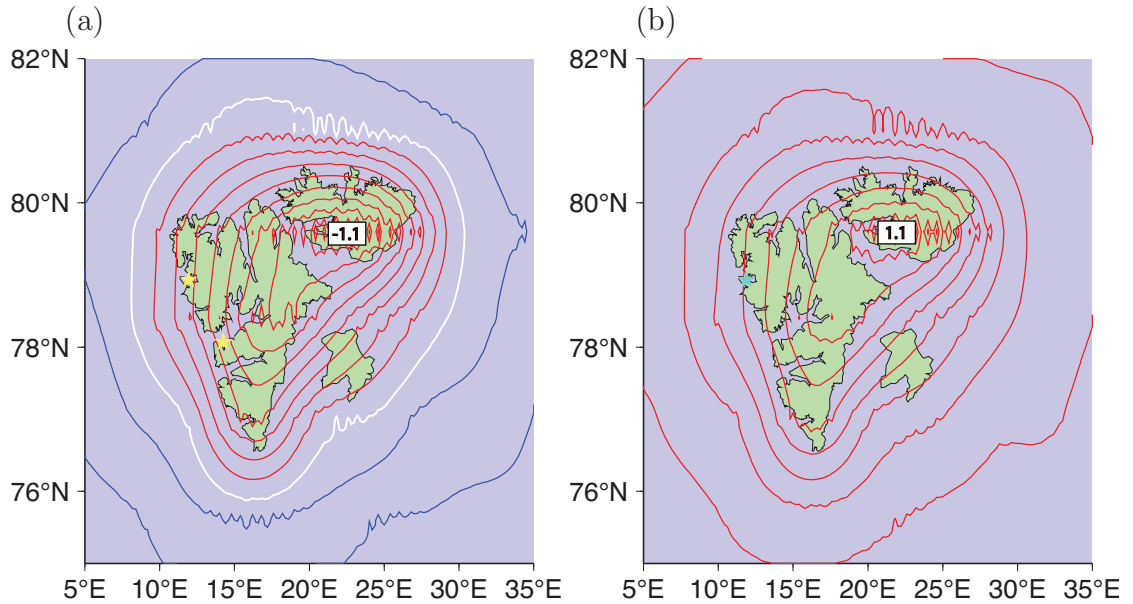
Figure 7.18: Spatial distribution of geodetic signals in Svalbard over the period 1961-2003 applying the D&M compilation of recent mountain deglaciation. The response is calculated on the standard Earth model $ma2A$. The contour interval is 0.1 mm year^{-1}. Numbers refer to the local maximum rates in mm year^{-1}. (a) Relative sea-level changes. Red contour lines represent relative sea-level fall, blue contour lines represent relative sea-level rise. White represents the zero contour line (no change). Stars indicate the locations of tide gauge sites of the PSMSL. (b) Vertical surface displacements. Red contour lines represent vertical land uplift (the outermost contour line represents 0.1 mm year^{-1}). The star indicates the location of the GPS and VLBI station.

Site	$T_G P_{Z\&O}$ 1961-1990	$T_{OF} P_{OFseries}$ 1961-2000	D&M comp. 1961-2003
Tide gauge:			
Ny Ålesund	-1.19	-1.04	-0.71
Barentsburg	-0.77	-0.67	-0.38
GPS / VLBI:			
Ny Ålesund	1.02	1.00	0.75

Table 7.9: Predictions of geodetic signals in mm year^{-1} at tide gauge and GPS/VLBI stations (see Tables D.1 and D.2) in Svalbard due to recent mountain deglaciation using the standard Earth model $ma2A$. Ice-volume changes are derived from the numerical model based on $T_G P_{Z\&O}$ and $T_{OF} P_{OFseries}$ (with a global Θ of 0.15 K) and from the estimates of the D&M compilation. Geodetic signals are averaged over the periods 1961-1990, 1961-2000, and 1961-2003.
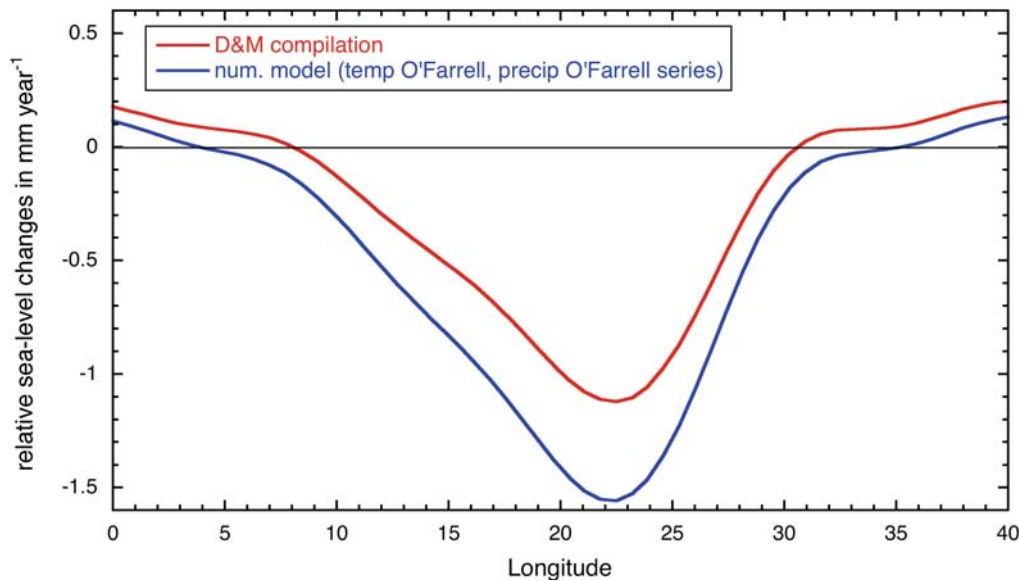
Figure 7.19: Cross-section of relative sea-level changes along 79.6ºN due to recent mountain deglaciation using two different global models, i.e. the numerical model based on $T_{OF}P_{OFseries}$ (with a global Θ of 0.15 K) and the D&M compilation.

the strong dependence of the predicted geodetic signals on the local ice models used. Another factor that contributed to the higher rates in relative sea-level fall is the slightly smaller eustatic contribution when derived numerically compared to that of the D&M compilation (see e.g. Figure 3.10 on page 99). This is also reflected in Figure 7.19, i.e. in the bias between the two curves seen well outside the extents of the load (between approximately 11 and 26ºE) where the deformational and gravitational components are less dominant (Section 4.3).

7.3.2 Geodetic signals from the study of Hagedoorn and Wolf (2003)

Hagedoorn and Wolf (2003) determined relative sea-level changes and vertical land uplift rates for the Ny Ålesund site on the Svalbard archipelago as a response to past glacial fluctuations. Comparing the method of calculating geodetic signals in Hagedoorn and Wolf (2003) with the one derived in this thesis reveals differences in the ice-volume changes and the Earth model used.

In Hagedoorn and Wolf (2003), the regional ice model accounting for the recent ice-volume loss in Svalbard is based on studies of mass balances of Hagen and Listøl (1990), Hagen (1996), and Dowdeswell et al. (1997), which are averaged to produce a mean value. This mean specific mass balance rate of -357 mm year^{-1} results

in a volume loss of $\sim$13 km^3 year^{-1} w.e. (equivalent to 0.036 mm year^{-1} global sea-level rise) assuming a total glacial area in Svalbard of 36,600 km^2. The mass balance measurements analysed in the three above studies cover time periods only within the second half of the 20th century. Hence, in Hagedoorn and Wolf (2003) the recent loading history starts in 1950 but they also produced a model where the ice-volume loss is extrapolated back to 1900. In contrast, the numerical model developed in this thesis produces a loading history over the period 1871-2000 and hence is expected to represent a better estimation of the ice-volume changes over the earlier half of the 20th century than the simple extrapolation undertaken in Hagedoorn and Wolf (2003). Calculating the ice-volume changes in Svalbard from the numerical model based on $T_{OF}P_{OFseries}$ results in a loss of 6.89 km^3 year^{-1} w.e. (equivalent to 0.019 mm year^{-1} global sea-level rise) over the period 1961-2000. Although this ice-volume loss is in agreement with the average estimate of the D&M compilation (as discussed in Section 7.3.1), it is only about half that of Hagedoorn and Wolf (2003). However, as already noted in Section 3.2.4.2, when using regionally variable Θs in the numerical model (which is estimated to be 0.85 K for the Arctic region, see Section 3.1.5), the resulting ice-volume loss in Svalbard is estimated to be 12.79 km^3 year^{-1} w.e. (equivalent to 0.035 mm year^{-1} global sea-level rise) over the period 1961-2000, and thus is in excellent agreement with that of Hagedoorn and Wolf (2003).

Differences in the predictions of geodetic signals between using the globally uniform Θ and regionally variable Θs can be examined by comparing column *2* with *4* in Table 7.10 (for this purpose the Earth model applied remained the same). This illustrates once more the strong dependence of geodetic signals on local ice-volume loss, i.e. the predicted geodetic rates double, similar to the rate at which the ice-volume loss increases.

The spatial distribution of the glaciated regions in Svalbard is simplified for the analyses in Hagedoorn and Wolf (2003), in particular they represent the ice loss by 15 ellipsoids. In contrast, in this thesis the extents of the ice cover in Svalbard were digitised (see Section 2.3.1.2) and therefore provide a better representation of the spatial distribution of their changes. Consequently, geodetic signals using the digitised data set can be estimated more accurately as the predictions are sensitive to the position of the site relative to the location of the load (see Section 5.2).

In order to calculate the Earth's response to glacial fluctuations, Hagedoorn and Wolf (2003) developed Earth models which include different parameters for the viscosity of the asthenosphere. The range of Earth models are similar to those

used in Lambeck (1995a), Kaufmann and Wolf (1996), and Kaufmann and Wu (1998). Only the study of Kaufmann and Wolf (1996) concluded that a range for the asthenospheric viscosity of 10^{18} to 10^{20} Pa-s is consistent with observations found at locations close to the continental margin, while the other two studies do not attempt any rigourous comparison with observational data. However, the existence of a low viscosity asthenosphere beneath Svalbard is still questionable. The study on postglacial rebound by Lambeck (1996) used improved ice models for Scandinavia and the Barents Sea (Lambeck, 1995b) and subsequently was able to explain the geological observations when Earth models with upper mantle viscosity of $> 10^{20}$ Pa-s are used (Lambeck et al., 1990; Lambeck, 1993). As a low viscosity zone ($< 10^{20}$ Pa-s) in the Earth results in a faster relaxation in case of surface loading or unloading, it is doubtful that such an Earth model can explain the observations of Late glacial and early Holocene raised shorelines in Svalbard.

The thickness of the layers and their viscosities, assuming the mid-range model of Hagedoorn and Wolf (2003), are illustrated in Figure 7.20. For comparison purposes, the Earth model *mdbw47* (Table 4.2 on page 117) with similar parameters to those suggested by Hagedoorn and Wolf (2003) has been developed in this thesis. Columns *2* and *3* of Table 7.10 compare estimates of geodetic signals at the Ny Ålesund site using the same recent deglaciation model but different Earth models. It illustrates that using an Earth model with a low viscosity asthenosphere results in greater rates of geodetic signals by about 35%.
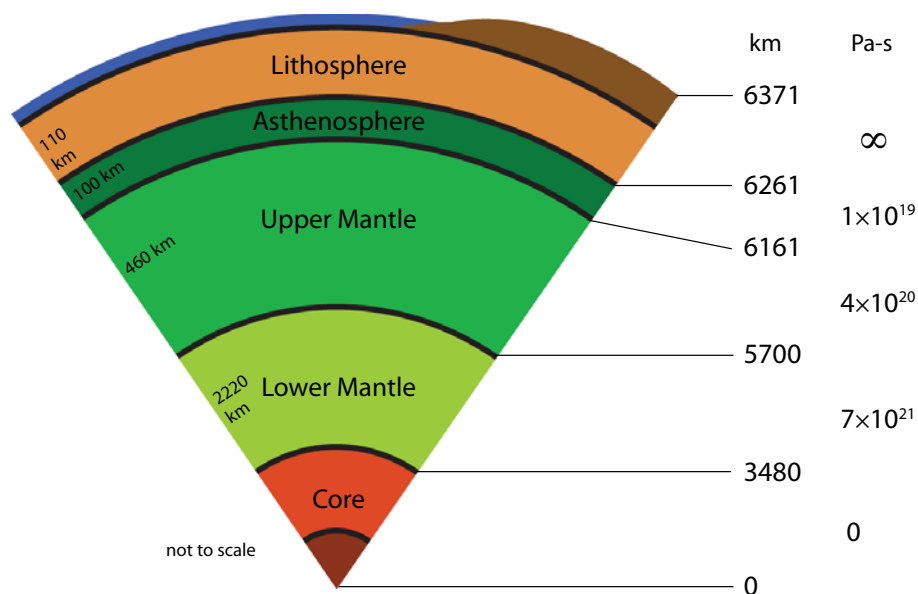

Figure 7.20: Parameters of layer thicknesses and mantle viscosities for the Earth model used by Hagedoorn and Wolf (2003).

The Pleistocene ice model ICE-3G of Tushingham and Peltier (1991) was adopted in the Hagedoorn and Wolf (2003) study to account for any remaining contributions to present-day geodetic signals from the melting of past ice sheets. Furthermore, Hagedoorn and Wolf (2003) developed a glaciation history in Svalbard for the time between the end of the Pleistocene, 11,000 years ago, and the start of the recent loading history (1900 or 1950). In Section 6.3.1 a model representing the glaciation/deglaciation cycles prior to and following the LGM was introduced and is available for this study. In Hagedoorn and Wolf (2003), the Earth's response to past glaciation/deglaciation cycles is calculated on the global Earth model MF2 of Mitrovica and Forte (1997) as this model represents the global rheology of the Earth better than the local model with a low viscosity asthenosphere. The mantle viscosity of the MF2 model is not lower than 10^{20} Pa-s and hence of the same order as those three-layer models used in this thesis (Section 4.2.1). It was shown in Section 6.3.1 that the present-day geodetic signal as a result of past deglaciation histories is predicted to be small at the Ny Ålesund site, in particular a relative sea-level rise of 0.44 mm year^{-1} and a vertical surface deformation of -0.24 mm year^{-1} are estimated (see also column *6* in Table 7.10).

The relative sea-level changes modelled by Hagedoorn and Wolf (2003) for the station Ny Ålesund range between -2.93 and -9.21 mm year^{-1}, depending on the Earth- and ice models applied. For an Earth model with an asthenospheric viscosity of 10^{19} Pa-s and a recent loading history starting in 1900, their estimated rate of relative sea-level change at the station Ny Ålesund is -5.11 mm year^{-1}. For the same Earth- and ice models, Hagedoorn and Wolf (2003) determined a vertical land uplift of 4.25 mm year^{-1} at the GPS station in Ny Ålesund (column *8* of Table 7.10).

The predicted geodetic signals over the period 1991-2000 (this interval was chosen as it corresponds roughly with the period for which observations are available) at the Ny Ålesund site using the adjusted Earth- and ice models developed in this section are listed in column *5* of Table 7.10. Considering the contribution to present-day geodetic signals from the melting of past ice-sheets (column *6*), resulting rates (column *7*) are only about half those determined by Hagedoorn and Wolf (2003) which are shown in *8* in Table 7.10.

According to Hagedoorn and Wolf (2003) tide gauge records at the Ny Ålesund site show a sea-level rate of -2.6 ± 0.7 mm year^{-1}. This number is derived from hourly values (over the period from 1992 to 1999) corrected for the inverted-barometer effect. In regards to vertical land movements in Svalbard, Hagedoorn and Wolf

(2003) presented a VLBI-derived uplift rate of 5.7±1.8 mm year^{-1}. Observations at the two GPS stations of the IGS network indicate a land uplift at a rate of 6.3±0.3 and 4.9±1.54 mm year^{-1}, respectively. The difference in the estimates at the two GPS sites (located in close proximity to each other) is due to the different time intervals that they have been in operation (installation in 1992 and 1998, respectively). The VLBI station has been in operation since 1994. Hagedoorn and Wolf (2003) concluded that their predicted uplift rate determined by a combined Earth and ice model matches the measured land uplift. However, with the same model their predicted relative sea-level fall is too high by approximately 3 mm year^{-1}. They concluded that this discrepancy may indicate a sea-level rise due to increased water volume of the oceans.

As for analyses in earlier sections, the contribution to sea-level changes resulting from thermal expansion of the oceans can be extracted from Levitus et al. (2005, Figure 1) or Antonov et al. (2005, Figure 4), where rates are predicted to be less than −0.4 mm year^{-1} for the North Atlantic (at around 80ºN) over the second half of the 20th century. As the results presented here are calculated over the period 1991-2000, a more representative estimate of the contribution to sea-level changes due to thermal expansion over the specific decade is required. This can theoretically be extracted from the work of Ishii et al. (2006) who presents the geographical distribution of sea-level changes (that is caused by ocean thermal expansion only) over the period 1993-2003. Although difficult to read and extrapolate, Ishii et al. (2006) estimated a trend for the Svalbard region of between −1 and +1 mm year^{-1}, i.e. essentially zero (see also Figure 5.15(b) in Bindoff et al., 2007). In total, the predicted sea-level change due to glacial unloading (column *7* in Table 7.10) is in agreement with the observation made at the tide gauge site (column *9* in Table 7.10).

In conclusion, the observations of relative sea-level changes and vertical surface deformation in Svalbard can only be partially explained by the numerical model of recent mountain deglaciation derived in this thesis. Considering the contribution from the deglaciation following the LGM, adjusting the Earth model (as suggested by Hagedoorn and Wolf, 2003), and adding the effect of thermal expansion do not always improve the agreement between predicted values and observations.

Another contribution to the geodetic signals which may improve the predictions (especially in light of the results given in the previous sections for the example of Alaska) is the prevailing response to major glacial fluctuations during and after the LIA. However, required information on these earlier glacial fluctuations for the

1	2	3	4	5	6	7	8	9
Ny Ålesund	num. deglaciation model based on $T_{OF}P_{OFseries}$				LGM	sum of columns 5 and 6	H&W	obs.
	$\Theta_{Svalbard}$ = 0.15 K		$\Theta_{Svalbard}$ = 0.85 K					
	ma2A	*mdbw47*	*ma2A*	*mdbw47*				
tide gauge	−1.11	−1.53	−2.44	−3.25	+0.44	−2.81	−5.11	−2.6±0.7
GPS nyal	1.13	1.55	2.22	3.04	−0.24	+2.80	4.25	6.30±0.30
GPS nyal								4.90±1.54
VLBI								5.70±1.80

Table 7.10: Estimates of geodetic signals in Svalbard in mm year^{-1} over the period 1991-2000. Columns 2 to 5 show predicted estimates determined from the numerical model based on $T_{OF}P_{OFseries}$. The parameter Θ is set to 0.15 K globally (columns 2 and 3) and the regionally variable Θs are also applied, where the value for Svalbard is 0.85 K (columns 4 and 5). The response is calculated on the *ma2A* and *mdbw47* Earth models. Column 6 lists the contribution as a result of past glaciation/deglaciation histories prior to and following the LGM. Column 7 lists the sum of the previous two colums, showing the total modelled geodetic signals due to past and recent glacial unloading/loading. The numerical estimates derived by Hagedoorn and Wolf (2003) are shown in column 8 and observations at the GPS and tide gauge sites in column 9.

Svalbard archipelago are not available (see also Section 6.3.2) and hence estimates can not be calculated. Tectonic movements can also play a major role in terms of geodetic signals (see Section 6.1), but are probably negligible in Svalbard since this area is tectonically relative inactive (Mitchell et al., 1990). Furthermore, the relatively short period with available observations at this site (in particular for the tide gauge site) rises the question whether the records exhibit a decadal variability that is not part of the long-term trend of the sea-level signal.

7.4   Summary and conclusions

As shown in Chapter 3, ice-volume changes derived numerically are comparable to estimates based on observational data, at least on a global scale and particularly over the second half of the 20th century. However, this chapter demonstrates that on a regional scale, exemplified by Alaska and Svalbard, the numerical model of mountain deglaciation may need to be recalibrated to match the observational based estimates. In the case of Alaska, this has been achieved by changing the parameter Θ to 0.50 K in the numerical model of mountain deglaciation based on combinations of temperature and precipitation data sets. Additionally, local variations in deglaciation histories (i.e. in Glacier Bay and of the Yakutat Icefield) need to be included to accommodate specific circumstances in this region.

It seems that the observational based estimates of ice-volume loss in Svalbard is poorly constrained, as the two studies of Hagedoorn and Wolf (2003) and Dyurgerov and Meier (2005) result in different rates of ice-volume loss (by a factor of two) over the second half of the 20th century. Hence, two different parameter settings used in the numerical model (a Θ of 0.15 and 0.85 K for Svalbard) result in predictions that are comparable with the observational based estimates.

In addition to the adjustments made to the ice models, some studies presented in this chapter suggest that a different Earth model should be used in the two regions compared to the one applied so far (standard Earth model). In particular, Earth models with a low viscosity asthenosphere were proposed by these previously published studies. Whereas in Alaska this adjustment may be adequate to account for local variations in the Earth rheology, it remains questionable whether a low viscosity asthenosphere is present beneath the Svalbard archipelago.

Subsequently, geodetic signals were calculated with the adjusted ice- and Earth models and hence are believed to be more accurately estimated now. It has been

demonstrated in this chapter, that the contribution of geodetic signals over the past few decades due to recent mountain deglaciation can be significant. However, it seems that the geodetic observations are still considerably contaminated by other processes since the numerically derived predictions of geodetic signals rarely match observations closely. In particular, most of the predicted rates are only about half the observational value. Reasons for that include the inadequately modelled (or completely ignored) effects of past ice sheets (following the LGM and LIA) due to restrictions of the required data sets, global ocean-volume changes due to other sources (e.g. thermal expansion), and recent tectonic activity. All these effects are addressed in this chapter but they may still be not accurately constrained at present.